Characterising the effects of shape on tool path motion

Chanda, Luke; Cripps, Robert

DOI:
10.1016/j.ijmachtools.2018.04.005

Document Version
Peer reviewed version

Citation for published version (Harvard):
Chanda, L & Cripps, R 2018, 'Characterising the effects of shape on tool path motion', *International Journal of Machine Tools and Manufacture*. https://doi.org/10.1016/j.ijmachtools.2018.04.005

Accepted Manuscript

Characterising the effects of shape on tool path motion

Luke Chanda, Robert J. Cripps

PII: S0890-6955(18)30082-8

DOI: 10.1016/j.ijmachtools.2018.04.005

Reference: MTM 3341

To appear in: *International Journal of Machine Tools and Manufacture*

Received Date: 11 December 2017

Revised Date: 16 April 2018

Accepted Date: 17 April 2018

Please cite this article as: L. Chanda, R.J. Cripps, Characterising the effects of shape on tool path motion, *International Journal of Machine Tools and Manufacture* (2018), doi: 10.1016/j.ijmachtools.2018.04.005.

Characterising the effects of shape on tool path motion

Abstract

This paper presents a methodology for *a priori* shape characterisation of tool path motion. Many current methods to describing tool path motion require explicit knowledge of the motion control algorithms implemented on a specific machine. Either a method proposes novel algorithms or requires knowledge of the algorithms currently implemented in a given machine's controller (e.g. minimum jerk, harmonic jerk and minimum jounce). This paper provides a method, that may be applied on any machine, to characterise motion in terms of a tool path's intrinsic shape properties. The characterisation identifies the achievable set of kinematics for a tool path of a given shape without the need for physical machining and a knowledge of the motion control algorithms. The characterisation may be employed in a pre-processing manner to inform the selection of NC file tool path motions. This can therefore help to reduce the material and energy resources being consumed during iterative machining trials and so improve the efficiency and productivity of the manufacturing process.

Keywords: tool path; shape; kinematics

1. Introduction

To manufacture computer-aided design (CAD) models, computer-aided manufacturing (CAM) software can produce commands for computer numerically controlled (CNC) machines. Integral parts of these commands are descriptions of desired motions of the cutting tool relative to the workpiece. Such descriptions are commonly referred to as tool paths. In general, tool paths are discretised and presented to a machine's controller as a locus of poses. A single pose defines a tool's position and orientation. A tool path can also be considered as a locus

of positions when a desired motion does not require changes in orientation.

A controller attempts to interpolate discretised tool paths by coordinating motion of independent translational and/or rotational axes. Linear and circular interpolation has traditionally been employed [1]. Piecewise-impulse and constant curvature profiles of such interpolated tool paths, can severely impede realisation of optimal kinematics and quality of the resulting machined component [2, 3].

Consider a tangent discontinuous tool path composed of linear segments. The tangent vector at the junction of consecutive segments is not unique. A singularity in the tool paths curvature function exists at such a point. This corresponds to instantaneous change in direction, which is not possible in practice. To follow the path exactly, the cutting tool must come to rest at the junction. This intermittent motion requires changes in acceleration. The rate of change of acceleration, with respect to time, is defined as jerk [4]. The jerk experienced in such a motion can change resultant forces on the cutting tool, resulting in deflection marks on the surface of the machined component [5]. Also, fluctuations in feed rate, acceleration and jerk increase numerical control cycle time and in turn reduce productivity [6].

To reduce fluctuations in kinematic properties of tool path motion, CNC controllers can permit the actual path to deviate from tangent discontinuous junctions by a given tolerance [6]. By accelerating drives that will be active in the next segment and decelerating drives that are currently moving, the cutting tool is able to bypass a junction with a feed rate greater than zero. The greater the commanded feed rate, the greater deviation required to ensure kinematic limits of a given machine are not exceeded. The precise nature of the deviating motion may not be known to the user.

Due to machine manufacturers having ownership to the motion control algorithms implemented in controllers, their specifics are indeed not generally accessible to the engineers using the CNC machines [7]. It is for this reason that the effects of controller regulation on tool path motions are generally identified after numerous machining trials. To initially specify tool path motion

parameters, such as feed rate and spindle speed, engineers therefore rely upon the recommendations of cutting tool manufacturers. These suggested values are however often based on assumptions of simple components with tool paths describing simple motions, predominately linear. Paths with varying curvature profiles, referred to in this paper as free-form paths, place a greater burden on control algorithms to generate the resulting motions.

Kinematics imposed by the shape of a free-form path, may exceed the capabilities of a given machine. For example, to maintain a specified feed rate, a machine must provide at each point, an acceleration proportional to curvature. If unachievable, a machine's controller must moderate axes motions to provide permissible kinematics. In general a reduced feed rate is observed.

For a given application, the autonomous regulation of kinematics by a controller may produce undesirable and unknown machining conditions. A commanded feed rate may have been specified to achieve particular conditions, for example specific material removal rates or surface finish. NC file tool path motions may therefore need to be *optimised* for the given application. In such instances machinist experience can be significant [8].

The optimisation methods employed may be iterative and informed by empirical evidence from machining trials. Such *a posteriori* attempts to obtain suitable tool path motions are often heuristic and time intensive. Prior knowledge of the effects of specified NC file tool path motions, on the actual machine motions, can inform their selection. This in turn may reduce the time and number of machining trials thereby increasing the efficiency of the machining process.

It should be noted that knowledge of a specific motion algorithm only enables tool path motion description for the machine upon which it is used. The main contribution of this paper is that it proposes a methodology that may be employed on any machine tool in order to obtain a suitable description of tool path motion without the need for physical machining or knowledge of the control algorithms implemented in the given machine's controller. The resulting description of tool path motion depends only upon the intrinsic shape properties

of a desired tool path and the kinematic limits of the given machine. Both these parameters are of the few conditions that are indentifiable without undergoing the iterative machining trial procedure. The paper therefore provides *a priori* shape characterisation of tool path motion. The characterisation may be employed to inform the selection of machining parameters and thereby reduce the time and the number of machining trials.

Currently, the primary means of describing tool path motion prior to physical machining is to acquire knowledge of the motion algorithms implemented in the machine's controller. However, as stated above, the algorithms are often not generally accessible. This has not deterred academia from proposing their own novel algorithms.

In general the proposed algorithms moderate both the commanded feed rate and tool path shape specified in the NC file in order to adhere to the machine's kinematic limits [9]. An algorithm may first fit a *smoother* path that interpolates the discrete NC file tool path poses whilst still adhering to the desired positional tolerances and then schedule an appropriate feed rate profile for the path's traversal [9].

Consider again the tangent discontinuous linearly segmented tool path. In order to combat the impractical kinematic demands imposed by the path's shape, a control algorithm may replace the junction between consecutive linear segments with a circular arc [6]. The direction of the tangent vector no longer changes instantaneously, thus enabling a continuous feed rate profile. Despite the revised tool path improving the motion, in the sense that traversal no longer requires an infinite acceleration, constant feed rate motion still cannot be realised. Although the imposed infinite acceleration has been removed, the new tool path's piecewise constant curvature imposes infinite jerk at the beginning and end of the arc. Attempts to produce these instantaneous changes in acceleration can excite vibrations in the mechanical structure of a machine and in turn degrade the dynamic performance of the servomotors [10]. It has been shown that constraining the permissible jerk experienced by each axis can limit the oscillatory behaviour of a machine and thus produce *smoother* tool

path motions [11]. Thus many motion control algorithms consider limited-jerk, minimum-jerk and harmonic-jerk movement laws [11–13]. Further by constraining the magnitude of the resultant jerk vector the cutting tool may follow the revised tool path exactly [12, 13].

Non Uniform Rational Basis Spline (NURBS) tool paths can also be implemented directly on many modern controllers. Motion control algorithms may use NURBS tool paths to avoid the impractical kinematic demands of linear and circular segments [14–17]. For example, two quartic polynomial splines can be used to achieve continuous curvature cornering within user specified tolerances [14]. A single G^2 quintic Bézier can be used to ensure axis acceleration limits are adhered to [15]. Many other proposed algorithms use B-splines as they offer flexibility in locally changing the shape of a tool path [16, 17]. However, the polynomial nature of NURBS means that tool paths can experience undulating oscillations in curvature which in turn impose fluctuations in the kinematic properties of tool path motion [7, 18].

As stated above, a key disadvantage of the current approaches is that they are only applicable to the given machines upon which the algorithms are implemented. The following sections of this paper describe and discuss an approach that may be employed on any machine in order to obtain a suitable characterisation of tool path motion without the need for physical machining or knowledge of the machine's motion control algorithms. Section 2 presents a description of machine motion in terms of tool path shape. Section 3 considers effects of kinematic limits on resulting motion. A Hermle C600U machine tool is then investigated as an example. First, in section 4, its kinematic limits are established by considering circular motions. Next, in section 5, planar spirals are traversed to consider the Hermle's behaviour to free-form path traversal. Section 6 details effects of shape in light of research undertaken. Finally, section 7 draws conclusions from key findings and suggests an area for future research.

2. Shape properties of motion

2.1. Local frame

The path traversed by a specified point on a cutting tool during a given motion can be represented as a parametric space curve, $\mathbf{r}(u)$, where u is an arbitrary parameter [19]. Assuming the path is continuous and differentiable, analysis of motion can be simplified by expressing it as a vector valued, time, t, parameterised function, in three dimensional Euclidean space, $\mathbb{E}^3$. $\mathbf{r}(t) = \langle x(t),\ y(t),\ z(t)\rangle$, $0 \leq t \leq T$, $x(t)$, $y(t)$ and $z(t) \in \mathbb{R}$ and T is the total time for the motion.

Employing a local coordinate system called the Frenet frame may facilitate describing each point in terms of shape properties of a tool path [18]. Considering changes in frame orientation as time increases can provide insight into effects of shape on tool path motion. As time increases it is assumed that the distance travelled along the path, arc length, s, increases monotonically. By reparameterising the path to arc length, frame motion may be expressed in terms of the path's intrinsic shape properties. Also a reparameterisation does not change the shape of the tool path. It then follows that $\mathbf{r}(s) \equiv \mathbf{r}(t)$, assuming $s = s(t)$ is differentiable and the inverse $t = t(s)$ exists. By letting $s(t) = \int \left\|\dot{\mathbf{r}}(t)\right\| dt$ be such a parameterisation,

$$\frac{d\hat{\mathbf{t}}(s)}{ds} = \kappa(s)\hat{\mathbf{n}}(s) \ , \tag{1}$$

$$\frac{d\hat{\mathbf{n}}(s)}{ds} = -\kappa(s)\hat{\mathbf{t}}(s) + \tau(s)\hat{\mathbf{b}}(s) \ , \tag{2}$$

and

$$\frac{d\hat{\mathbf{b}}(s)}{ds} = -\tau(s)\hat{\mathbf{n}}(s) \ . \tag{3}$$

In Eqs. 1, 2 and 3, $\hat{\mathbf{t}}(s)$, $\hat{\mathbf{n}}(s)$ and $\hat{\mathbf{b}}(s)$ are defined as the unit tangent, principal normal and binormal vectors respectively and functions $\kappa(s)$ and $\tau(s)$ refer to shape properties curvature and torsion respectively [20]. Formally $\kappa(s)$ and

$\tau(s)$ are defined by Eqs. (1) and (3) respectively. They can also be considered to describe frame motion and in turn any object that moves with the frame, for example a cutting tool. As a Frenet frame traverses a path, $\kappa(s)$ and $-\tau(s)$ describe the angular velocities of unit tangent and binormal vectors [18]. Further, curvature and torsion are independent of path parameterisation. They are euclidean invariants and more over, they uniquely define a tool path's shape.

Arc length parameterisation of tool paths provides a means of describing tool path motion in terms of intrinsic shape properties, curvature and torsion. Such descriptions are machine independent. The corresponding kinematic demands on a machine's motors can therefore be expressed without reference to a machine's coordinate system. Only tool path shape and commanded feed rate are required to describe the velocity, $\mathbf{v}(t)$, acceleration, $\mathbf{a}(t)$ and jerk, $\mathbf{j}(t)$, imposed on a machine's servo motors.

2.2. Velocity vector

The derivative of position vector, $\mathbf{r}(s)$, with respect to time, t, produces the velocity vector, $\mathbf{v}(t)$,

$$\mathbf{v}(t) = \frac{d}{dt}\{\mathbf{r}(s)\} \ .$$

The magnitude of this vector quantifies the rate at which the arc length of a tool path changes with respect to time. In the context of machining, the magnitude of velocity is perhaps more appropriately referred to as feed rate. The vector describes the rate at which a tool is moving relative to a tool path in the direction of a linear curve, having first order contact with the tool path. In general, an arc length parameterised curve of order n, having n^{th} order of contact to the tool path at a given point, is defined as a n^{th} order osculant [20]. For the velocity vector, the osculant is a line that best approximates the path in the vicinity of a given point

$$\mathbf{v}(t) = \frac{ds}{dt}\frac{d\mathbf{r}(s)}{ds} \ .$$

Therefore,

$$\mathbf{v}(t) = \frac{ds}{dt}\hat{\mathbf{t}}(s) \ . \tag{4}$$

2.3. Acceleration vector

The derivative of velocity vector, $\mathbf{v}(t)$, with respect to time, t, produces the acceleration vector, $\mathbf{a}(t)$. Therefore,

$$\mathbf{a}(t) = \frac{d}{dt}\left\{\frac{ds}{dt}\hat{\mathbf{t}}(s)\right\}$$

$$= \frac{d^2s}{dt^2}\hat{\mathbf{t}}(s) + \left\{\frac{ds}{dt}\right\}^2 \frac{d\hat{\mathbf{t}}(s)}{ds} \ .$$

Substituting Eq. (1) into the above equation produces an expression for the acceleration vector in terms of its tangent and normal components:

$$\mathbf{a}(t) = \frac{d^2s}{dt^2}\hat{\mathbf{t}}(s) + \left\{\frac{ds}{dt}\right\}^2 \kappa(s)\hat{\mathbf{n}}(s) \ . \tag{5}$$

The tangential component describes the rate of change of feed rate with respect to time. The normal component may be interpreted geometrically in terms of curvature. Its magnitude is proportional to the rate at which the unit tangent vector changes direction with respect to arc length. At a given point the normal component acts towards the centre of the circle of curvature [20]. This circle is a second order osculant at each point on the path. Its derivatives, up to and including order two, agree with those of the path [20]. The normal acceleration component is therefore commonly referred to as *centripetal* (centre seeking) acceleration [21]. Eq. (5) shows that it consists of a time dependent and a shape dependent element, feed rate, ds/dt, and curvature, $\kappa(s)$, respectively. To illustrate the effect of each element on centripetal acceleration, $a_n(t)$, the normal component of Eq. (5) may be visualised as a surface expressed explicitly in terms of ds/dt and $\kappa(s)$, $a_n(t) = (ds/dt)^2\kappa(s)$ (Fig. 1). For a constant feed rate, ζ, centripetal acceleration increases linearly with curvature, $a_n(t) =$

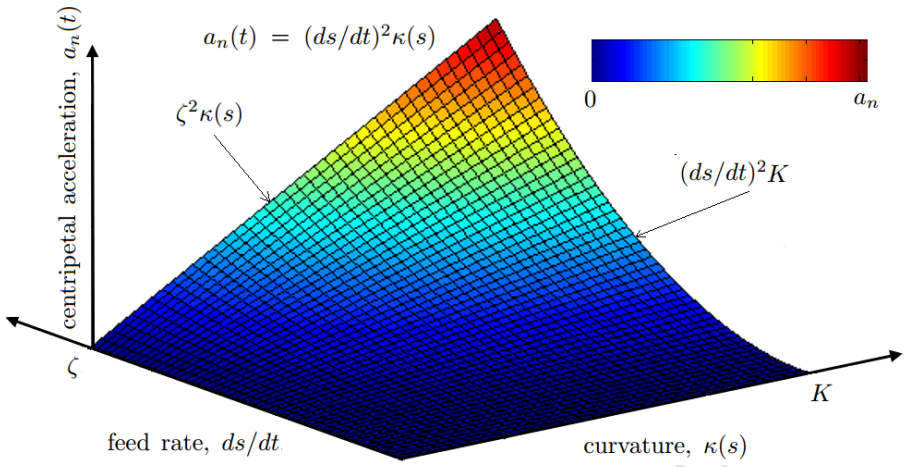

Figure 1: Centripetal acceleration surface

$\zeta^2\kappa(s)$ (Fig. 1). For a constant curvature, K, centripetal acceleration increases parabolically with feed rate, $a_n(t) = (ds/dt)^2K$ (Fig. 1).

2.4. Jerk vector

Jerk has perhaps received comparatively little attention since it does not appear in mathematical expressions of fundamental engineering concepts likes energy, force and momentum. However, trends of high speed machining and increased part shape complexity, have lead to jerk becoming an important parameter that should be well considered [7]. Jerk has been shown to influence vibrations of industrial high-speed systems [22]. Significant research has been conducted to consider jerk when planning machine tool motion [9, 23–25]. The affects of shape on this kinematic property are therefore described below.

Taking the derivative of Eq. (5) with respect to time and making substitutions with Frenet-Serret formulae it can be shown that jerk can be described as the sum of three orthogonal components (See Appendix B).

$$\mathbf{j}(t) = j_t(t)\hat{\mathbf{t}}(s) + j_n(t)\hat{\mathbf{n}}(s) + j_b(t)\hat{\mathbf{b}}(s) \; ; \tag{6}$$

where

$$j_t(t) = \frac{d^3s}{dt^3} - \left\{\frac{ds}{dt}\right\}^3 \{\kappa(s)\}^2 \ ,$$

$$j_n(t) = 3\frac{ds}{dt}\frac{d^2s}{dt^2}\kappa(s) + \left\{\frac{ds}{dt}\right\}^3 \frac{d\kappa(s)}{ds} \ ,$$

and

$$j_b(t) = \left\{\frac{ds}{dt}\right\}^3 \kappa(s)\tau(s) \ .$$

Just as the normal component of acceleration can be expressed in terms of curvature, the normal component of jerk can be expressed in terms of a higher affine differential invariant of plane paths, namely *aberrancy* [26]. Aberrancy is a measure of local asymmetry of a path with respect to a path's normal at a given point [26]. It can be shown that the normal component of jerk, at a given point on a path, is related to a third order osculant called the osculating parabola. This is a unique parabola whose Cartesian derivatives, up to and including order three, agree with those of the path [4].

2.5. Kinematic demands

This section shows, curvature and torsion are intrinsically related to velocity, acceleration and jerk. It follows that tool path shape imposes particular kinematic demands on a machine's motors [7]. In practice, a given machine's motors are only supplied with finite amount of electrical energy. Some of this electrical energy is converted, with losses, into mechanical energy in order for the motors to produce limited power and torque in their attempt to provide the desired motion. For example, motors must provide sufficient power to overcome machine inertia, cutting forces and friction [2]. The kinematic demands resulting from tool path shape also correspond to specific energy requirements. If these requirements exceed physical capabilities of motors, specified motions may be compromised.

3. Bounded motion

3.1. Kinematic limits

The specific nature of how a given machine may regulate its kinematic performance is often the intellectual property of machine and controller manufacturers. This section characterises, in terms of intrinsic shape properties, possible planar motion ($\tau(s) = 0$) behaviour a machine may adopt in order to adhere to kinematic limits. Two distinct phases of kinematic behaviour are considered. First, motion at the commanded feed rate, Ψ_1, is considered. Such motion is defined as velocity limited phase motion. Second, the magnitude of the centripetal acceleration vector is constrained to Ψ_2. The resulting effects on the kinematics vectors of tool path motion are defined as acceleration limited phase motion. For example, Fig. 2 shows that at (κ_α, Ψ_1) the commanded feed rate is no longer achieved and as a result of the enforced constraint on the centripetal acceleration vector, the feed rate must decrease.

3.2. Velocity limited phase

To maintain a specified feed rate, Ψ_1, along a tool path, a machine must produce the required kinematics (velocity, acceleration, jerk, etc.). A constant feed rate implies the velocity vector is

$$\mathbf{v}(t) = \Psi_1 \hat{\mathbf{t}}(s) \ . \tag{7}$$

If $ds/dt = \Psi_1$ it follows that,

$$\frac{d^2 s}{dt^2} = \frac{d^3 s}{dt^3} = 0 \ .$$

There is therefore no tangential acceleration for constant feed rate traversal. The acceleration vector then lies solely normal to the direction of travel. Eq. (5) thus becomes,

$$\mathbf{a}(t) = \Psi_1^2 \kappa(s) \hat{\mathbf{n}}(s) \ . \tag{8}$$

Given constant feed rate, the jerk vector (Eq. (6)) becomes,

$$\mathbf{j}(t) = \Psi_1^3 \Big[\frac{d\kappa(s)}{ds} \hat{\mathbf{n}}(s) - \{\kappa(s)\}^2 \hat{\mathbf{t}}(s) \Big] \ . \tag{9}$$

3.3. Acceleration limited phase

To prevent a machine's centripetal acceleration exceeding it's bound, Ψ_2, the controller may regulate motion. A possible action is to continue to provide maximum centripetal acceleration despite curvature imposing a greater magnitude. The curvature at which kinematic behaviour transitions between phases, referred to in this paper as *transition curvature*, κ_α, can be identified from the normal component of Eq. (5). It follows $\kappa_\alpha = \Psi_2/\Psi_1^2$. During the acceleration limited phase:

$$\Big\{ \frac{ds}{dt} \Big\}^2 \kappa(s(t)) = \Psi_2 \ ,$$

and so,

$$ds/dt = \sqrt{\Psi_2/\kappa(s)} \ . \tag{10}$$

The magnitude of velocity is thus inversely proportional to the root of curvature,

$$\mathbf{v}(t) = \sqrt{\Psi_2/\kappa(s)} \hat{\mathbf{t}}(s) \ . \tag{11}$$

A tangential deceleration must occur if feed rate reduces. The second derivative of arc length with respect to time provides an expression of the necessary tangential deceleration,

$$\frac{d^2 s}{dt^2} = -\frac{1}{2} \sqrt{\frac{\Psi_2}{\{\kappa(s)\}^3}} \frac{d\kappa(s)}{ds} \frac{ds}{dt} \ .$$

Because of Eq. (10), the tangential acceleration component can be expressed as

$$\frac{d^2 s}{dt^2} = -\frac{1}{2} \Psi_2 \frac{1}{\{\kappa(s)\}^2} \frac{d\kappa(s)}{ds} \ . \tag{12}$$

Thus the complete acceleration vector is given by

$$\mathbf{a}(t) = \Psi_2 \Big[\hat{\mathbf{n}}(s) - \frac{1}{2} \frac{1}{\{\kappa(s)\}^2} \frac{d\kappa(s)}{ds} \hat{\mathbf{t}}(s) \Big] \ . \tag{13}$$

The normal component of acceleration is constant by definition and Eq. (12) shows that the magnitude of the tangential component is inversely proportional to the square of the curvature of the tool path.

An expression for tangential jerk, $j_t(t)$, requires evaluation of the third derivative of arc length with respect to time (See Eq. (6)). It can be shown that (See Appendix C),

$$\frac{d^3 s}{dt^3} = -\frac{1}{2} \Psi_2 \sqrt{\Psi_2} \sqrt{\kappa(s)} \frac{1}{\{\kappa(s)\}^3} \left[\frac{d^2\kappa(s)}{ds^2} - 2 \frac{1}{\kappa(s)} \left\{ \frac{d\kappa(s)}{ds} \right\}^2 \right] \ .$$

Given that,

$$\left\{ \frac{ds}{dt} \right\}^3 \{\kappa(s)\}^2 = \Psi_2 \sqrt{\Psi_2} \sqrt{\kappa(s)} \ ,$$

it then follows that tangential jerk can be expressed as

$$j_t(t) = -\frac{\Psi_2 \sqrt{\Psi_2} \sqrt{\kappa(s)}}{2\{\kappa(s)\}^3} \left[\frac{d^2\kappa(s)}{ds^2} - 2 \frac{1}{\kappa(s)} \left\{ \frac{d\kappa(s)}{ds} \right\}^2 + 2\{\kappa(s)\}^3 \right] \ . \tag{14}$$

In general, the magnitude of the tangential jerk at the end of the velocity limited phase, $\jmath_V$, is not equal to the magnitude of the tangential jerk at the beginning of the acceleration limited phase, $\jmath_A$, $\jmath_V \neq \jmath_A$. This implies the jerk profile is discontinuous. The magnitude of this discontinuity, $|\jmath_V - \jmath_A|$, is dependent on kinematic limits of the given machine, feed rate and the rate at which curvature changes with respect to arc length.

Substituting Eqs. (10) and (12) into the expression for the normal component of jerk (Eq. (6)) replaces the time dependent elements (ds/dt and d^2s/dt^2) with corresponding shape elements ($\kappa(s)$ and $d\kappa(s)/ds$). It then follows that,

$$j_n(t) = -\frac{\Psi_2 \sqrt{\Psi_2} \sqrt{\kappa(s)}}{2\{\kappa(s)\}^2} \frac{d\kappa(s)}{ds} \ . \tag{15}$$

Having described the characteristics of bounded tool path motion in terms of shape, Eqs. (7–9), (11) and (13–15) are consolidated into a series of diagrams, referred to in this paper as *shape schematics* (Figs. 2, 3, 4 and 5).

Curvature alone describes the shape of a planar tool path [20]. By plotting the magnitude of each kinematic vector with respect to curvature, each of the shape schematics provide a complete illustration of the effects of planar tool path shape on a given kinematic vector. Further, by considering a constant curvature derivative, the shape of the profiles are independent of any derivative of curvature with respect to arc length, $d^n\kappa(s)/ds^n$, $n \geq 1$. Within the context of the schematics, these derivatives simply correspond to the rates at which the profiles are rendered. For simplicity, it is assumed that the schematics are rendered at a constant rate, specifically $d\kappa(s)/ds = 1 \Rightarrow d^n\kappa(s)/ds^n = 0$, $n \geq 2$.

In Fig. 3, γ_1 denotes the value of the instantaneous deceleration required tangential to the path as the motion transitions into the limited acceleration phase. γ_1 can be found by substituting κ_α into Eq. (12). Since $d^2s/dt^2\big|_{\kappa(s)=\kappa_\alpha} \equiv \gamma_1$ and $d\kappa(s)/ds = 1$,

$$\gamma_1 = -\frac{1}{2}\Psi_2\frac{1}{\kappa_\alpha^2} \quad .$$

In Fig. 4, γ_2 denotes the value of the instantaneous jerk required opposite to the direction of the principal unit normal vector, as the motion transitions into the limited acceleration phase. γ_2 can be found by evaluating Eq. (15) when $\kappa(s) = \kappa_\alpha$. It then follows that,

$$\gamma_2 = -\frac{\Psi_2\sqrt{\Psi_2}\sqrt{\kappa_\alpha}}{2\kappa_\alpha^2} \quad .$$

In Fig. 5 both γ_3 and γ_4 denote values of the tangential jerk at the transition curvature. If a given motion transitions from the velocity limited phase to the acceleration limited phase, the schematic shows the magnitude of tangential jerk changes instantaneously from $|\gamma_3|$ to $|\gamma_4|$. If a motion transitions from the acceleration limited phase to the velocity limited phase, the magnitude of tangential jerk changes instantaneously from $|\gamma_4|$ to $|\gamma_3|$. Considering the

tangential component of Eq. 9 it follows that,

$$\gamma_3 = -\Psi_1^3 \kappa_\alpha^2 \ .$$

γ_4 can be found from Eq. (14). Since $d\kappa(s)/ds = 1 \Rightarrow d^2\kappa(s)/ds^2 = 0$, therefore at the transition curvature, κ_α,

$$\gamma_4 = \Psi_2 \sqrt{\Psi_2} \left\{ \sqrt{\frac{1}{\kappa_\alpha^7}} - \sqrt{\kappa_\alpha} \right\} .$$

γ_5, in Fig. 5, denotes the point at which the direction of the tangential jerk vector changes again. This can be found by equating Eq. (14) to zero and accounting for $\kappa \geq \kappa_\alpha$.

Discontinuities present in the schematics arise from the idealised assumption of removing acceleration and deceleration from and to rest. In practice these discontinuities, that occur at the transition curvature, refer to the discrete time period where the machine transitions from one limited phase to another. The actual curvature at which this transition begins must therefore be less than the theoretical transition curvature.

4. Identifying kinematic limits

4.1. Strategy

Differences between requested and achieved kinematics for specified tool paths can be analysed to establish a given machine's limits. Circular motion is deemed appropriate to identify these limits. Since the paths are of constant curvature, kinematics imposed by shape remain constant throughout motion. Analysis of requested motion is further simplified as the paths are closed and so motion is periodic and can be characterised as simple harmonic motion (SHM). For constant feed rate ($ds/dt = v_c$) traversal of circular tool paths (let $\kappa(s) = \kappa_c$), Eqs. (4), (5) and (6) reduce to $\mathbf{v}(t) = v_c \hat{\mathbf{t}}(s)$, $\mathbf{a}(t) = v_c^2 \kappa_c \hat{\mathbf{n}}(s)$ and $\mathbf{j}(t) = v_c^3 \kappa_c^2 \hat{\mathbf{t}}(s)$ respectively. The magnitudes of velocity, acceleration and jerk can thus be quantified by establishing the feed rate achieved for a test tool path of a given curvature.

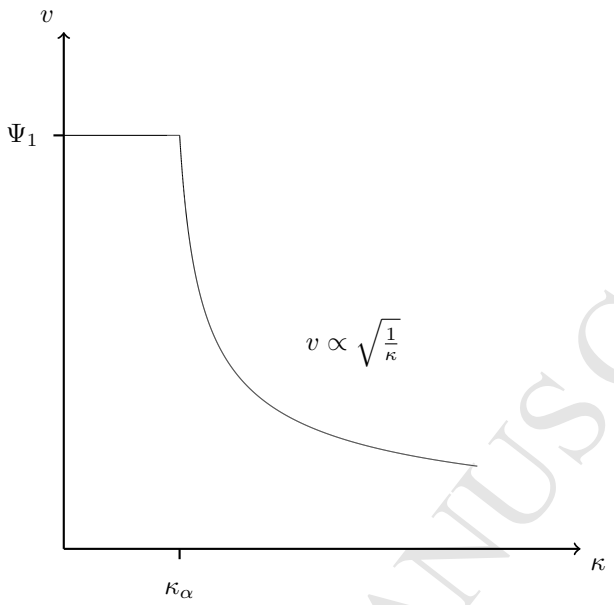

Figure 2: Velocity schematic

4.2. Data acquisition

As an example, the kinematic behaviour of a Hermle C600U machine tool (Fig. 6) is investigated. Using the machine's maximum feed rate ($35m/min$) for testing, ensures the highest kinematic demands are enforced on the machine for each circular path. It then follows that the achieved kinematics, on a given circular path, are the maximum attainable for the corresponding curvature.

The machine has a combination of 3 linear axes configured in a Cartesian coordinate system and a tilting rotary table. Circular motions are performed through simultaneous motion of 2 linear axes. The specific two linear axes chosen are immaterial. Each linear axis is orthogonal to the other two, therefore assuming each axis has the same kinematic capabilities, the kinematic properties of each axis form Cartesian components of the resultant kinematic properties of tool path motion. Technical data, presented in the literature for the machine, indicates that indeed all axes have the same kinematic specification [27].

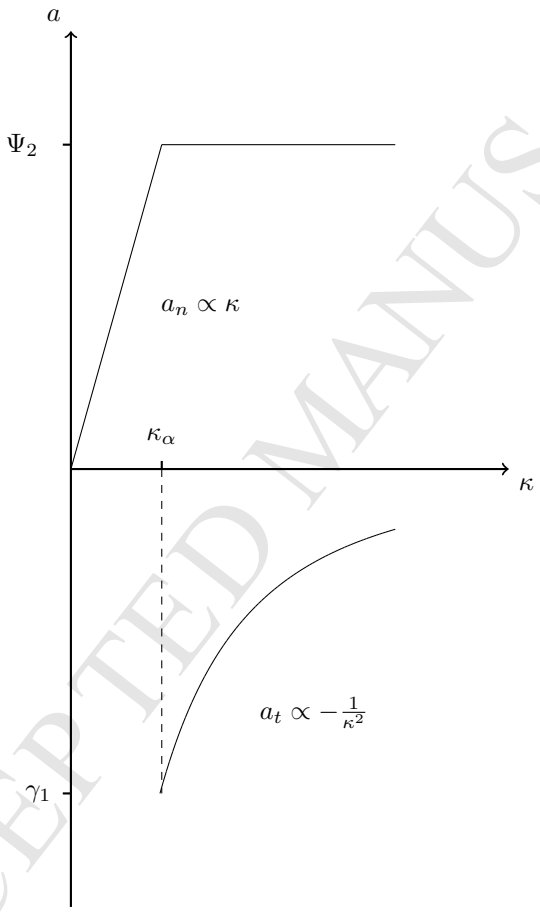

Figure 3: Acceleration schematic

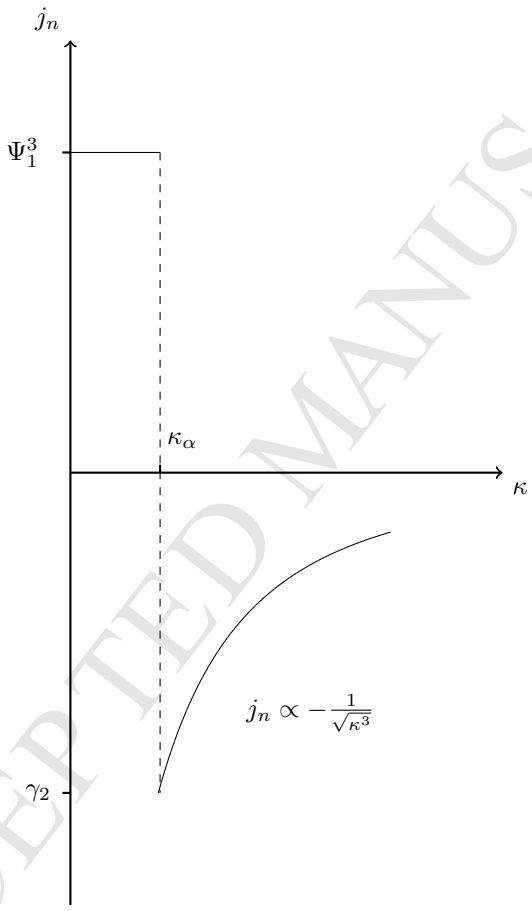

Figure 4: Normal jerk schematic

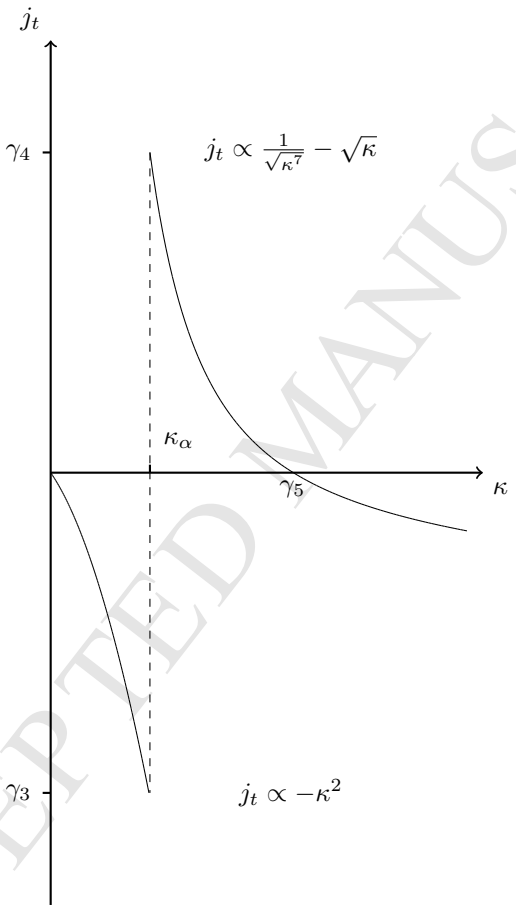

Figure 5: Tangential jerk schematic

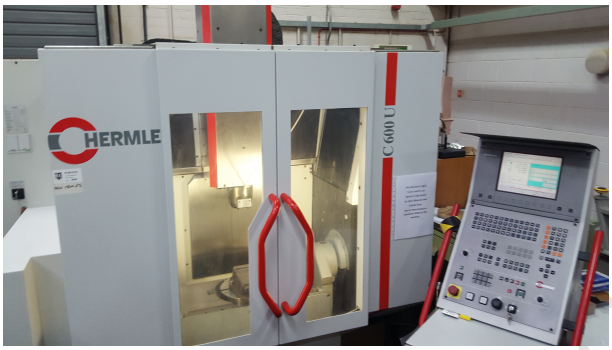

Figure 6: Hermle C600U

Performing multiple revolutions of a circular path can provide sufficient time for the digital read-out (DRO) of feed rate from the controller (TNC430A) to stablise. The DRO is therefore used as a preliminary indication of feed rate, v_{DRO}.

An inertial sensor, specifically a tri-axial accelerometer is used as an independent source of measurement. The main principle upon which the accelerometer operates is the piezoresistive effect [28]. This is a phenomenon whereby the application of mechanical stress causes a change in the electrical resistivity of a semiconductor material [29]. A Wheatstone-bridge configuration of piezoresistors measure and amplify this change in resistance and produce a voltage that is proportional to the acceleration experienced by the accelerometer and in turn, any object attached to it [30].

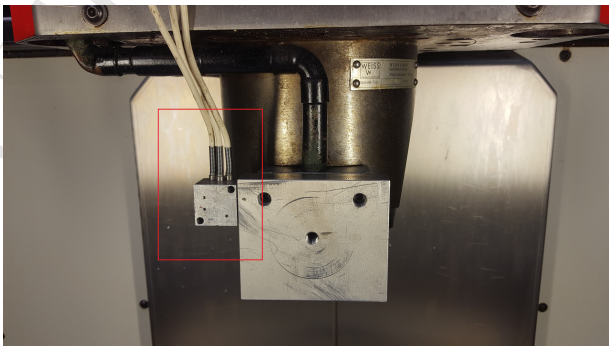

Figure 7: Tri-axial accelerometer

A *SoMat eDAQ-lite* data acquisition system (Fig. 8) is used to draw signals from the accelerometer and process data [31]. *SoMat Test Control Environment* (TCE) software is the interface through which setup, calibration and data retrieval is preformed [32].

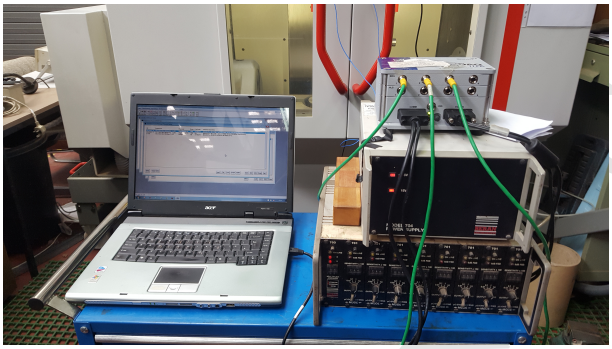

Figure 8: SoMat eDAQ-lite set up

4.3. Analysis

To remove contributions of accelerations from and to rest, multiple revolutions (5 revolutions) are preformed of each circular path and initial and final revolutions are ignored from analysis. Three different methods of quantifying kinematics for a given test are employed as a means of improving reliability of data.

From the controller's DRO of feed rate, v_{DRO}, the acceleration, $a_{DRO} = v_{DRO}^2 \kappa_c$ and jerk, $j_{DRO} = v_{DRO}^3 \kappa_c^2$, are deduced.

Using time data from the accelerometer, an average of the time periods, T_t, for intermediate revolutions is taken and since the length of each path, S, is known, an estimate to feed rate, $v_t = S/T_t$, can be obtained. Thus a measure of acceleration, $a_t = v_t^2 \kappa_c$ and jerk, $j_t = v_t^3 \kappa_c^2$, can be made. Similar approaches to quantify the kinematics of tool path motion from timings have also been employed in industry [33–35].

Output of the accelerometer is axes accelerations and motion times. The acceleration signals of a given test result from many contributing factors, including tool path shape. It can be shown that a given signal can be represented as a

collection of sinusoids [36]. Fourier analysis is used to identify characteristics (amplitude A, phase ϕ, frequency f) of each component sinusoid. This information is used to calculate time period, $T_{\mathbb{F}} = 1/f$, of a given circular motion and thus obtain the feed rate, $v_{\mathbb{F}} = S/T_{\mathbb{F}}$. The associated acceleration, $a_{\mathbb{F}}$, and jerk, $j_{\mathbb{F}}$, are given by $a_{\mathbb{F}} = v_{\mathbb{F}}^2 \kappa_c$ and $j_{\mathbb{F}} = v_{\mathbb{F}}^3 \kappa_c^2$.

To demonstrate Fourier analysis, consider traversal of a circular path of $1mm$ radius at a commanded feed rate of $35m/min$. Fig. 9 illustrates the acceleration profiles extracted from the accelerometer. To express a discrete acceleration signal, $a(t_i)$, of N samples, in the frequency domain, $\hat{a}(f_i)$, the following transform is used.

$$\hat{a}(k) = \sum_{j=1}^{N} a(j) W_N^{(j-1)(k-1)},$$

where W_N is a complex number and $W_N = e^{-\frac{2\pi i}{N}}$. Applying the transform to each axis acceleration profile ($a_x(t)$ and $a_y(t)$) allows each profile to be represented in the frequency domain ($\hat{a}_x(f)$ and $\hat{a}_y(f)$). Fig. 10 illustrates the frequencies and the relative amplitudes of the sinusoids present in each axis acceleration profile. Since tool path motion occurs without physical machining and surplus mechanical loading (e.g. cutting tool in the spindle), the dominant frequency in Fig. 10 maybe attributed to the acceleration signal imposed by tool path shape. This frequency may then be used to derive the time period of the given circular motion and the subsequent kinematic properties as described above.

Each of the three methods is applied to obtained the kinematics produced by the machine for each tool path. Figs. 11 and 12 summarise the results.

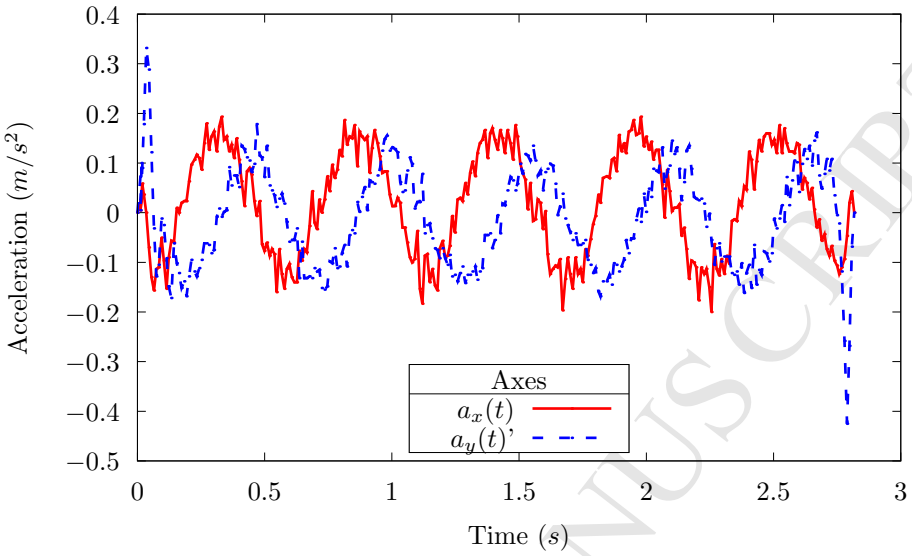

Figure 9: Axis accelerations (Radius $r = 1mm$)

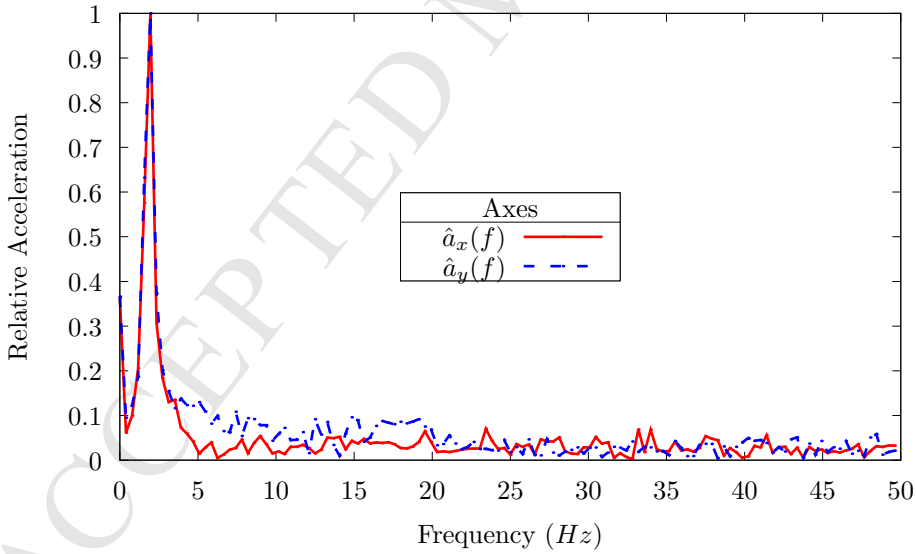

Figure 10: Component sinusoids within the signals

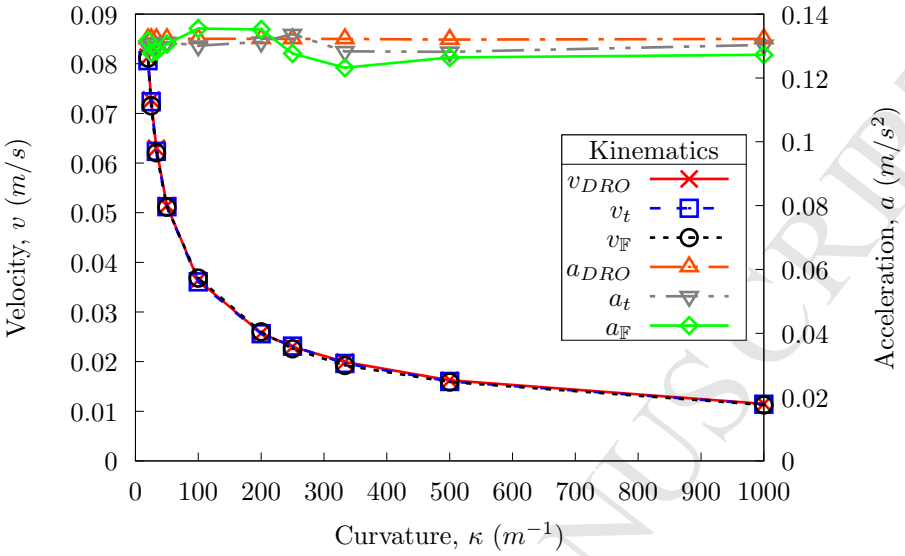

Figure 11: ALP - velocity and acceleration

The variation in magnitude of the centripetal acceleration, with respect to curvature, is considered negligible compared to the variation in achieved feed rate. The profiles then demonstrate the constant centripetal acceleration feature, upon which the characteristic model, given in section 3, is based.

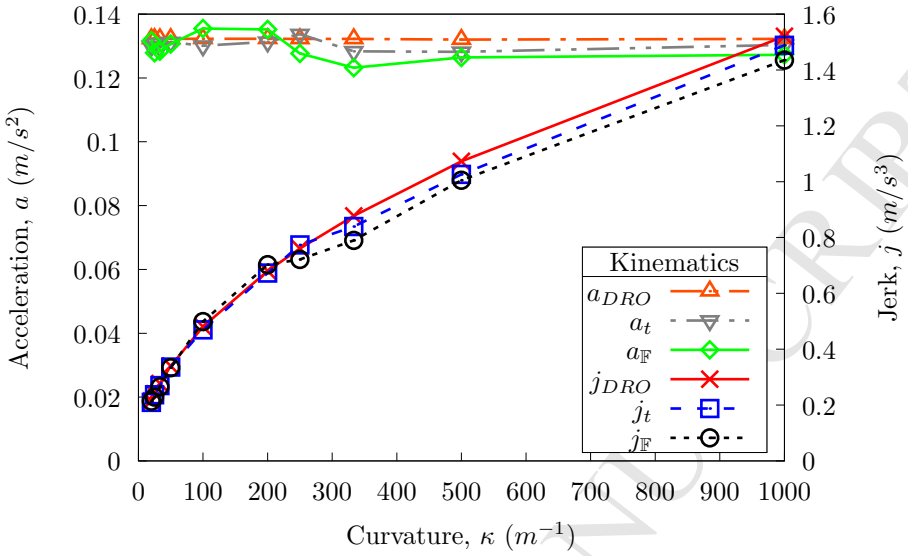

Figure 12: ALP - acceleration and jerk

The results suggest that, for the maximum commanded feed rate, centripetal accelerations imposed by curvatures of circular tool paths exceed the capabilities of the machine. The commanded feed rate is not achieved for any test tool path. Feed rate profiles (Fig. 11) resemble the schematic shown in section 3. The magnitudes of the centripetal accelerations remain constant, relative to the variations in magnitudes of velocity and jerk. Fig. 11 describes the maximum feed rate attainable by the machine for a given curvature.

A lower commanded feed rate is obtainable for paths whose curvatures do not impose a centripetal acceleration greater than the Hermle's limit. Fig. 13 demonstrates that a commanded feed rate of $F_c = 0.05\ m/s\ \equiv\ 3000\ mm/min$ is obtainable for four of the test tool paths, specifically paths of curvatures $\kappa = 20,\ 25,\ 33.\dot{3}$ and $50 m^{-1}$. Further, Fig. 14 shows the machine is able to provide the necessary centripetal accelerations and jerks in order to achieve the lower commanded feed rate. It should be noted that the specific value chosen for the lower commanded feed rate tests is immaterial. The only necessary condition is that it should be achievable for the test curvatures. Traversing a circle of curvature $33.\dot{3}\ m^{-1}$, at a commanded feed rate of $0.05\ m/s$, imposes a centripetal

acceleration of $0.08\dot{3}\ m/s^2$. As illustrated by empirical data presented in Fig. 11, such an acceleration is achievable and so the lower commanded feed rate can be achieved on the test path. It then follows that the feed rate can be achieved for the test tool paths with lower curvatures.

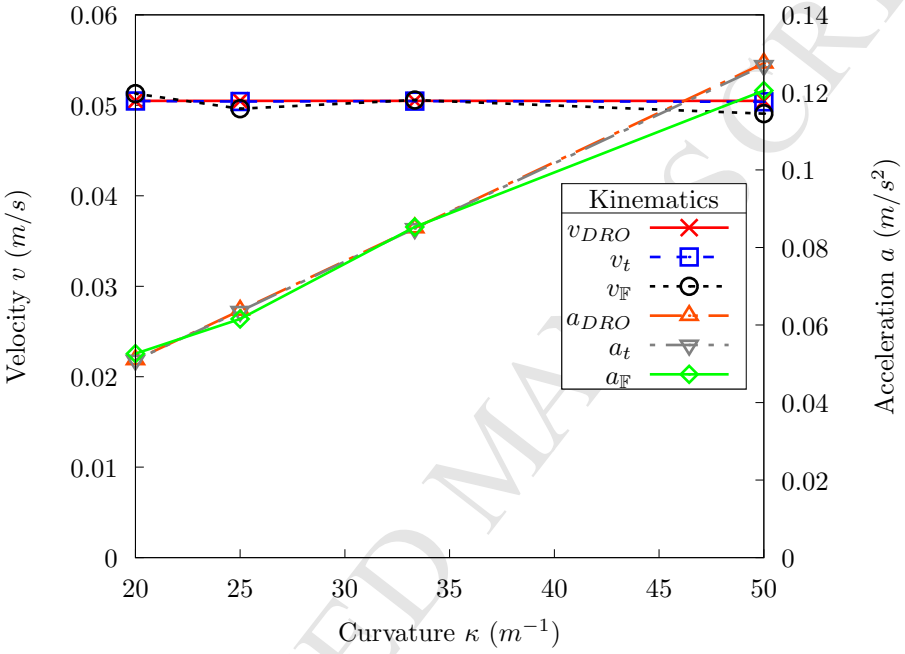

Figure 13: VLP - velocity and acceleration

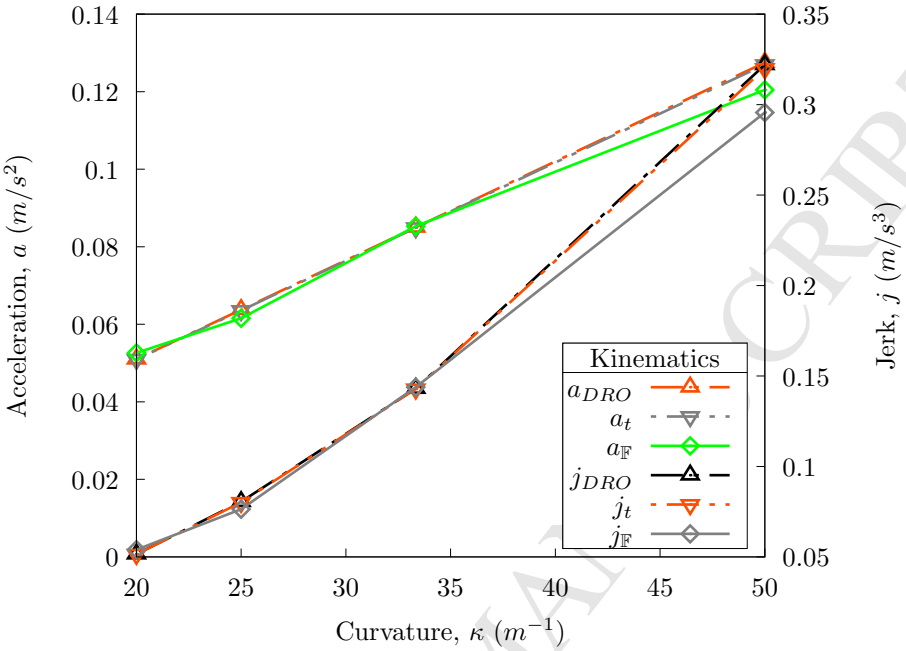

Figure 14: VLP - acceleration and jerk

5. Spiral path experiments

5.1. Cornu spiral tool path

Empirical data, presented in the previous section, suggests the Hermle's tool path motion can be characterised by equations developed in section 3. However, profiles in section 4 are derived from a number of constant curvature tool paths, not a single path with varying curvature. To further the investigation, kinematics produced from traversing a Cornu spiral path are analysed.

A Cornu spiral is a planar path, defined by a linear curvature profile $\kappa(s) = \alpha s + \beta$, $s \leq s \leq L$ and α, $\beta \in \mathbb{R}$ [37]. The path's curvature imposes a magnitude of centripetal acceleration that increases linearly with arc length (Eq. 5). By defining α, β and L such that the Hermle's transition curvature κ_α (see section 3.3) lies on the path, a change from the velocity limited phase to the acceleration limited phase may be observed. Further, since the curvature profile

is monotonic, empirical kinematic profiles may produce the same characteristic features as illustrated by Figs. 2, 3, 4 and 5.

In practice, a path with a linear curvature profile cannot be represented exactly in a NC file. Since paths of constant curvature can be represented exactly, linear and circular arc segmented tool paths are used to form approximations to a Cornu spiral's linear curvature. For both types of tool path, the segment lengths are kept constant (linear segment length is L_{line} and arc segment length is L_{arc}) and sufficiently long to negate influences of controller processing capability. The minimum segment length, s_{min}, is identified and verified by experimental data presented in Appendix A.

5.2. Path generation

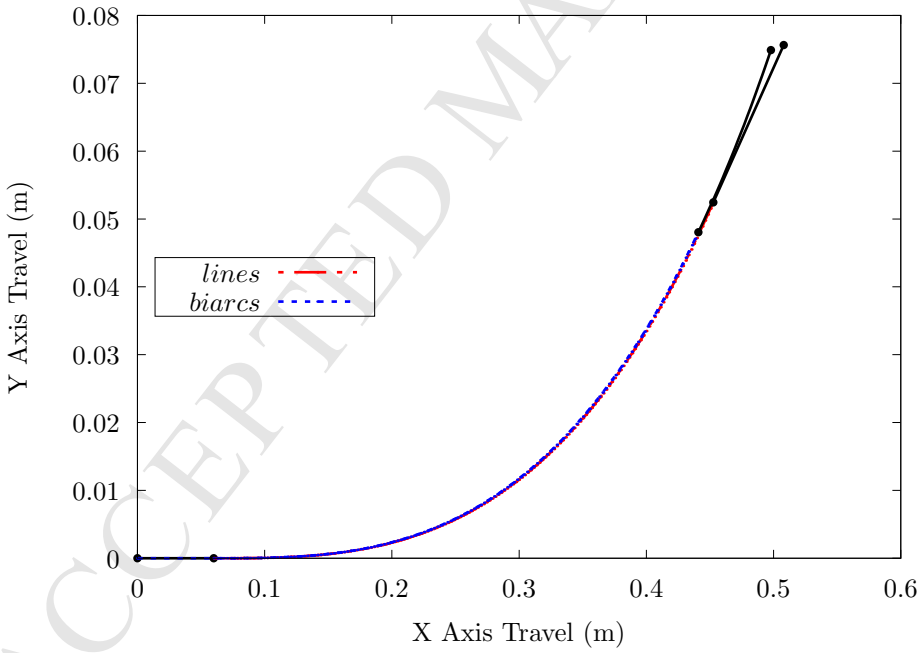

Figure 15: NC File Tool Paths

Linear segmentation. Eqs. (16) and (17) show that positions on a Cornu spiral path $(x(s),\ y(s))$ can be expressed in terms of it's curvature profile,

$$x(s) = x_0 + \int_0^s cos\Big[\theta_0 + \frac{1}{2L}\{2\kappa_0 L\sigma + (\kappa_1 - \kappa_0)\sigma^2\}\Big]d\sigma \ , \tag{16}$$

and

$$y(s) = y_0 + \int_0^s sin\Big[\theta_0 + \frac{1}{2L}\{2\kappa_0 L\sigma + (\kappa_1 - \kappa_0)\sigma^2\}\Big]d\sigma \ , \tag{17}$$

where (x_0, y_0) is the start of path, θ_0 is initial angle made the path with x-axis, L is the total length of path and κ_0 and κ_1 are initial and final path curvatures respectively [37]. The expressions contain transcendental functions called Fresnel integrals [38]. Numerical methods are therefore required to approximate curvature synthesis [39].

Some error may be present in the result due to the numerical nature of the approximation. Since the true value of a position is not knowable, the error in a given result cannot be stated. However it is possible to bound the error of numerical integration between two given limits, s_{min} and s_{max}. To simplify analysis of the error bound, ε_B, the trapezoidal rule is adopted for numerical integration [38]. The error bound can thus be given as

$$\varepsilon_B = -\frac{(s_{max} - s_{min})^3\{\kappa_0 L + (\kappa_1 - \kappa_0)s_{max}\}^2}{12N^2L^2} \ ,$$

where N is the number of segments in the given interval. The derivation of this error bound is provided in Appendix D. Provided the error is less than the positional accuracy of the given CNC machine, the positions form the closest representation of Cornu spiral path positions for the given machine.

The positions are linearly interpolated and since the curvature of a Cornu spiral changes strictly monotonically, consecutive linear segments join with position continuity, G^0. The result is an impulse curvature series that approximates a Cornu spiral's linear curvature profile. The diagram shown in Fig. 16 illustrates the approximation. Eq. (5) shows that at each joint in a linearly segmented spiral, the path shape imposes an infinite acceleration in the normal

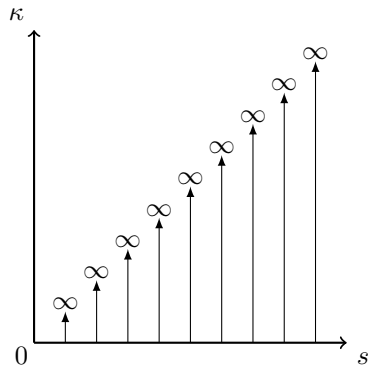

Figure 16: Piecewise impulse curvature profile

direction to the path, $|a_n(s)| = \infty$. Constant feed rate traversal cannot be achieved for such a path. The machine's controller may fluctuate feed rate in order to accommodate impractical demands of the tool path shape.

Biarc segmentation. Circular arcs are another type of constant curvature path that can be represented exactly. Connecting two circular arcs with tangent continuity, G^1, forms a composite curve known as a *biarc* [40]. By using biarcs, tangent continuity is achievable whilst still providing a path whose curvature can vary. To ensure tangent continuity, the centre of the second arc, $\mathbf{O}_{i+1}$, must lie on the line passing through the centre of the first arc, $\mathbf{O}_i$, and the end point of the first arc, $\mathbf{P}_{i+1}$. To generate an approximation to a Cornu spiral path the following scheme is employed (Fig. 18).

1. Rotate point $\mathbf{P}_i$ about centre $\mathbf{O}_i$ through angle $\theta_i = L_{arc}/r_i$.
2. Find new radius. $r_{i+1} = 1/(\alpha s_{i+1})$, where $s_{i+1} = s_i + L_{arc}$.
3. Find the new centre of rotation $\mathbf{O}_{i+1}$. $\mathbf{O}(r_{i+1}) = \mathbf{P}_{i+1} r_{i+1} + \mathbf{O}_i(\lambda - r_{i+1})$, where $\lambda = \|\mathbf{O}_i - \mathbf{P}_{i+1}\|$.

The result is a piecewise constant curvature series that approximates a Cornu spiral's linear curvature profile. The diagram shown in Fig. 17 illustrates the approximation. A step change in curvature corresponds to a point where two arc segments meet. The magnitude of curvature changes instantaneously from $1/r_i$ to $1/r_{i+1}$. Eq. (6) shows the shape of a biarc segmented spiral path imposes

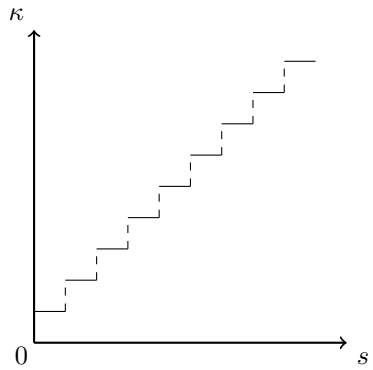

Figure 17: Piecewise constant curvature profile

an infinite jerk in the normal direction to the path, $|j_n(s)| = \infty$. This kinematic demand is not achievable. As with the linearly segmented spiral tool path, the biarc segmented spiral tool path requires a machine controller to comprise the requested motion and produce an alternative motion that its control algorithms deem appropriate.

Test paths. Both approximations generate paths whose shapes impose impractical kinematic demands. To investigate behaviour of the Hermle in response to these demands, a linearly segmented Cornu spiral path and a biarc segmented Cornu spiral path are traversed with the same commanded feed rate. The lower the chosen feed rate, the higher the path's curvature values need to be in order for the Hermle's centripetal acceleration limit to be exceeded. Practically, the selected feed rate and curvature profile must result in accelerations that can be measured by the chosen data acquisition system. Preliminary testing reveals that traversing the paths shown in Fig. 15, developed from the intrinsic equation $\kappa(s) = 2s$, $0 \leq s \leq 0.4m$, with a commanded feed rate of $0.5m/s \equiv 30m/min$, produces accelerations that can be measured by the triaxial accelerometer (Fig. 7). Further, as discussed above (section 5.1), the chosen combination of feed rate and tool path shape ensure that the corresponding transition curvature lies on the desired Cornu spiral path. Each tool path also has acceleration and deceleration segments, $0.06m$ in length (Fig. 15). They

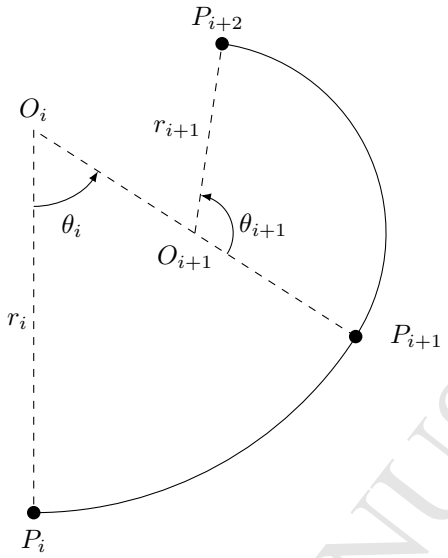

Figure 18: Biarc construction

ensure acceleration and deceleration from and to rest to occur outside the range of the test curvatures. These added segments join to their respective spiral paths with the same level of geometric continuity achieved by the rest of the path; G^0 for the linear segments approximation and G^1 for the biarc segments approximation.

5.3. Motion Analysis Methodology

The limits Ψ_1 and Ψ_2 are key kinematic attributes that define the bounded motion behaviour shown in section 3. These limits can be identified from profiles describing feed rate and normal acceleration performance with respect to curvature (Figs. 2 and 3). The feed rate and normal acceleration profiles from the spirals motions are therefore analysed in order to identify whether the Hermle exhibits the same bounded motion behaviour.

Data extracted from the accelerometer presents acceleration in terms of machine axis components $\mathbf{a_x}(t) = a_x(t)\hat{\mathbf{x}}_\mathbf{m}$ and $\mathbf{a_y}(t) = a_y(t)\hat{\mathbf{y}}_\mathbf{m}$. Achieved axes velocities and displacements are derived from axis acceleration profiles. Feed rate, normal acceleration and curvature can then be deduced.

The biarc approximation spiral tool path case is used to demonstrate the analysis procedure. Fig. 19 presents accelerations experienced by the Hermle's x and y axes.

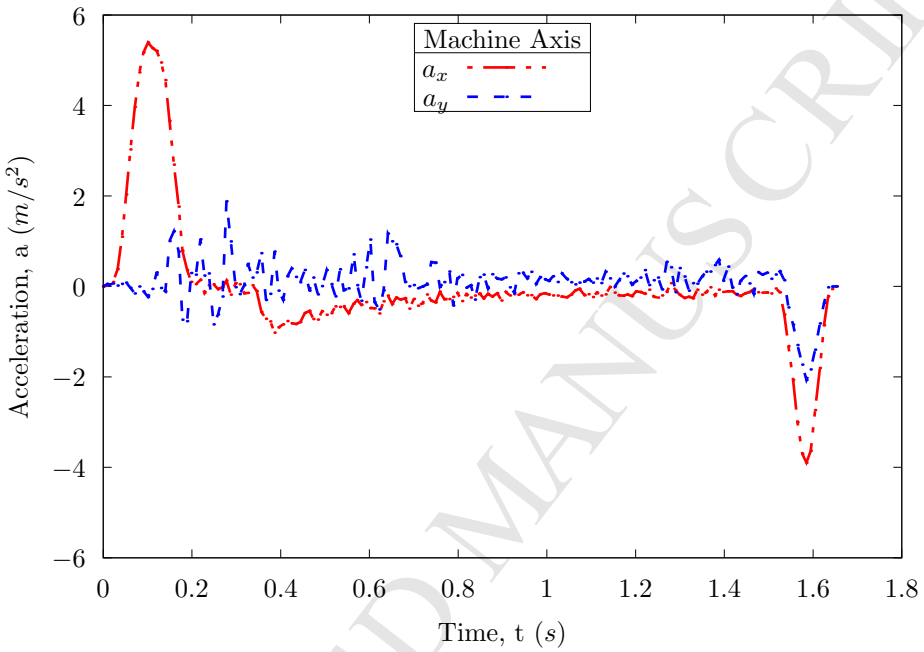

Figure 19: Biarc spiral acceleration profile

Integration of each axis acceleration component results in axis velocity. Each element of a discrete set of acceleration values may harbour some degree of error. This error is preserved through integration and as a result misrepresents velocity. Fig. 20 shows velocity resulting from integration of x-axis acceleration for biarc spiral path traversal. *Forward* integration from beginning $t = 0$ to the end of the motion $t = t_N$ produces velocity denoted by v_f. *Backward* integration from $t = t_N$ to $t = 0$ produces velocity denoted by v_b. Profile v_f suggests the x-axis changes direction towards the end of the path and profile v_b suggests the axis started the motion not from rest.

By cause of the cumulative nature of the integration process, the effects of the errors propagate through the definite integrals and culminate at end limits

of both the forward and backward integrations. Inherent error present in the acceleration signals, is combated by preforming a Hermite blend $H(v_f, v_b)$ of the resulting velocity profiles,

$$H(v_f, v_b) = v_f\left(1 - \frac{t}{t_N}\right) + v_b\left(\frac{t}{t_N}\right) .$$

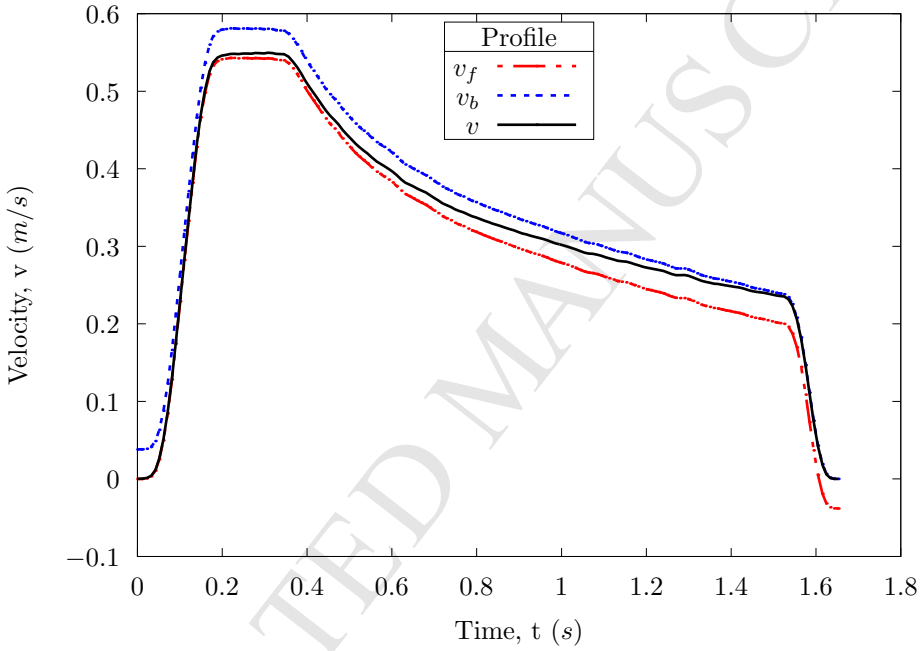

Figure 20: Blending

The euclidean norm of resulting axis velocities forms a representation of the feed rate profile, $v = \sqrt{v_x^2 + v_y^2}$ (Fig. 21).

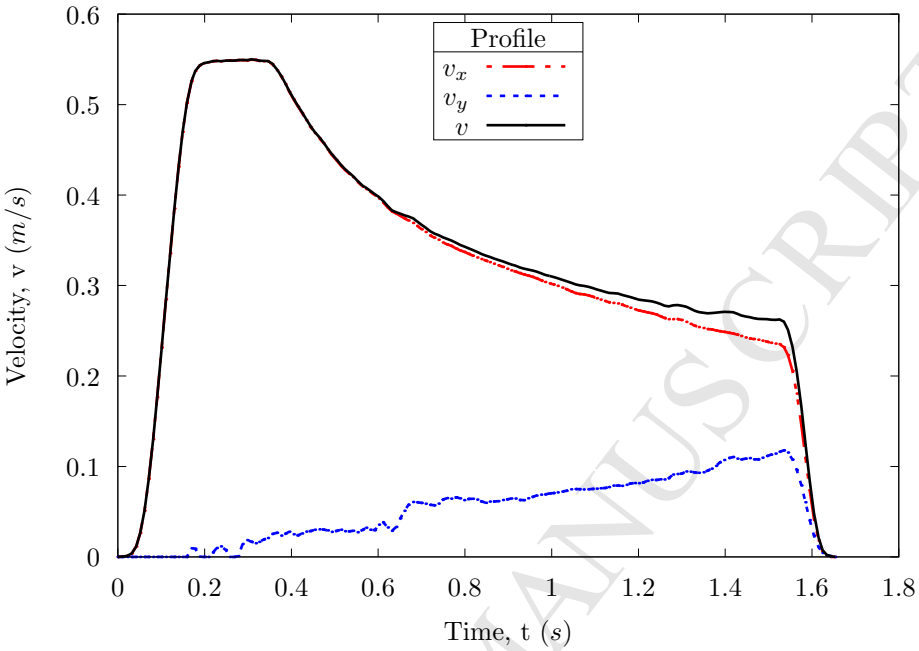

Figure 21: Axis velocities and feed rate

Axis displacements (Fig. 22) are derived by the same blending approach. From axis displacements arc length is found, $s = \sqrt{s_x^2 + s_y^2}$. An approximation to curvature is formed by scaling arc length by the specified rate of change of curvature ($\alpha = 2 \Rightarrow \kappa(s) = 2s$).

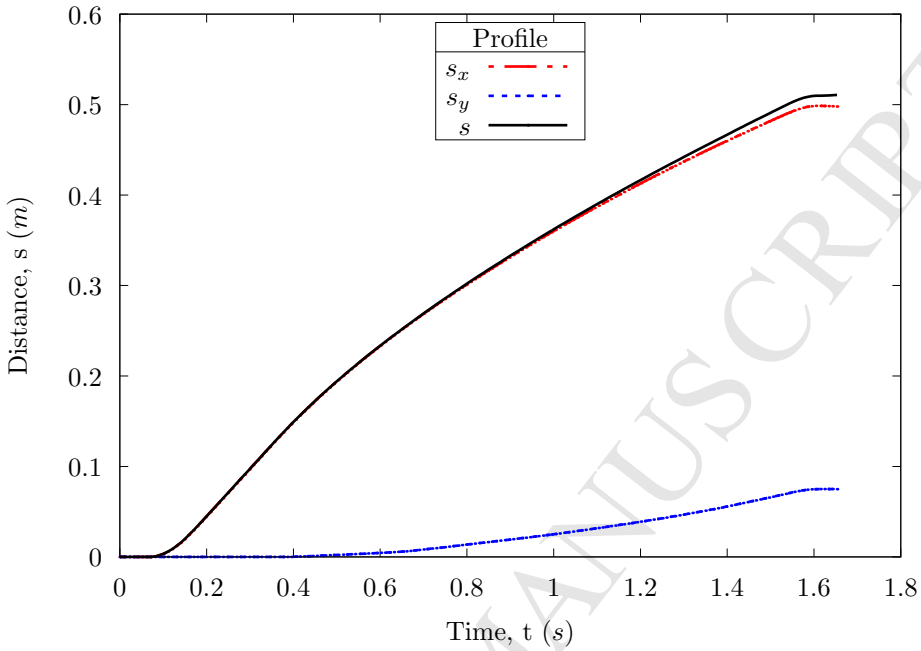

Figure 22: Axis displacements and arc length

5.4. G^0 vs. G^1 Spiral Motion Analysis

As with section 3, phases of acceleration and deceleration from and to rest are omitted from analysis. Fig. 23 shows feed rate resulting from traversals of linearly segmented, G^0, and the biarc segmented, G^1, spiral approximation tool paths. Both profiles may be considered to show two distinct types of kinematic behaviour. From $0 \leq \kappa \leq 0.16$ both profiles demonstrate relatively negligible feed rate variation. This suggests the motion may be characterised as limited velocity behaviour. The general trend of both profiles from $0.16 \leq \kappa \leq 0.8$ is for the feed rate to decrease as curvature increases. The nature of the decrease is characteristic of the limited acceleration behaviour described in section 3.

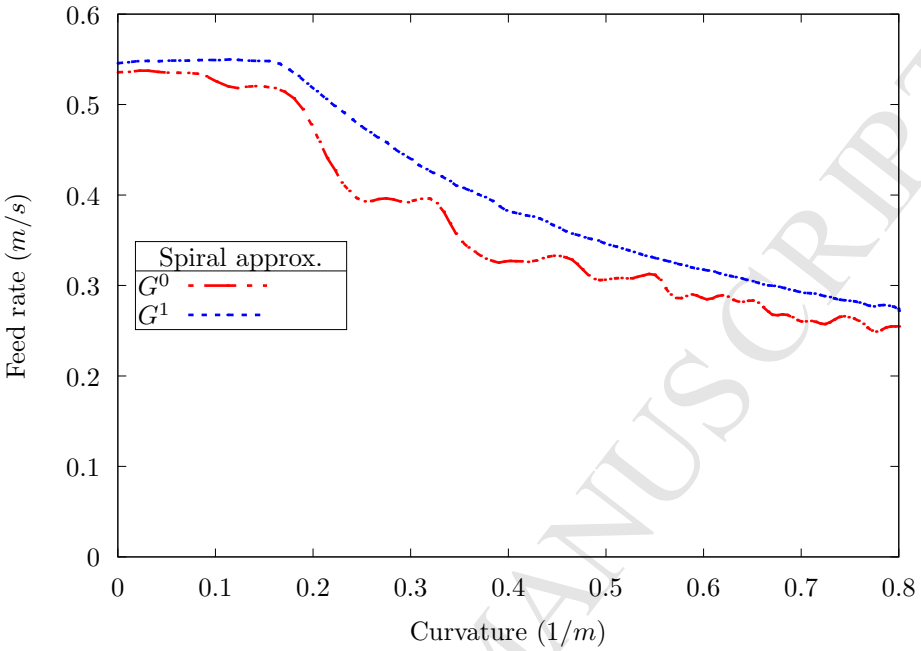

Figure 23: Feed rate

By substituting empirical feed rate values and appropriately scaled arc lengths values into Eq. (5), a set of normal component acceleration values can be obtained. Fig. 24 shows normal components of acceleration vectors, resulting from each tool path motion. Both demonstrate a transition from velocity limited to acceleration limited behaviour.

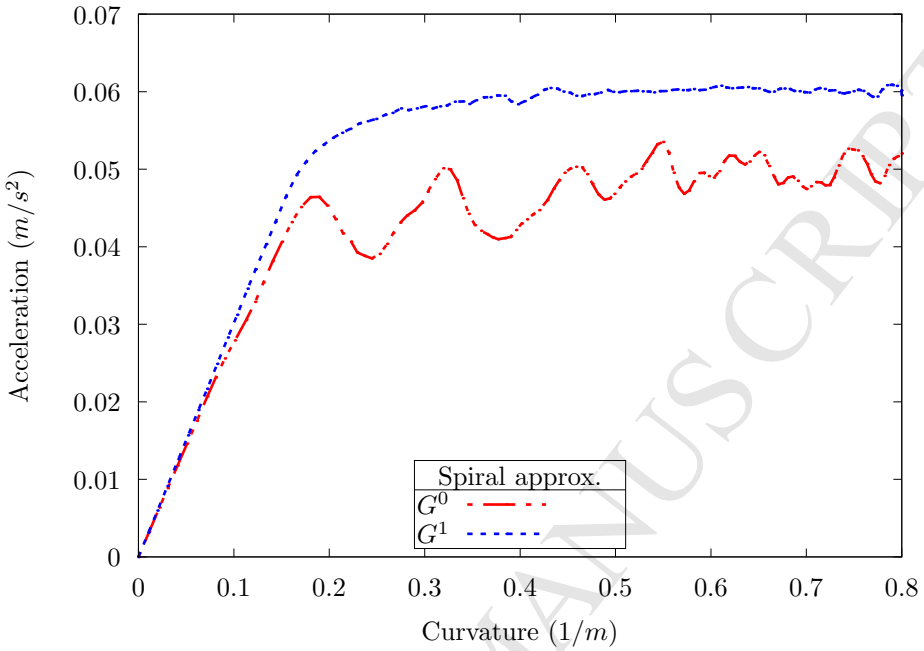

Figure 24: Normal acceleration component

6. Discussion

Both spiral approximation tool paths specify constant feed rate traversal in the NC files. Analysis of shape properties, undertaken in section 5, reveals both paths impose impractical kinematic demands in order to provide constant feed rate. Machine kinematic regulation is therefore required for motion. The results are provided by Figs. 23 and 24. Both profiles in Fig. 23 show lower attainable feed rates for higher path curvatures. This may perhaps be intuitive for many machinists. Yet by virtue of this investigation, relationships between tool path shape and machine motion can be further refined. For example, in the case of the Hermle C600U machine tool, it is demonstrated that feed rate is inversely proportional to the square root of curvature. Figs. 23 and 24 illustrates the machine's transition from limited velocity to limited acceleration behaviour. Both profiles, in Fig. 24, show initial periods of motion where centripetal acceleration rises linearly with curvature to maintain a constant feed rate. As the machine

transitions into the limited acceleration phase, acceleration no longer increases linearly and submits to the centripetal acceleration limit.

Comparing motions resulting from the segmented spirals highlights effects of shape on tool path motion. Tangent discontinuities may be considered to impose greater kinematic demands on machine motion than curvature discontinuities, since a lower order time derivative is undefined in the associated set of kinematic functions. Traversal of the linearly segmented spiral requires, at each segment junction, infinite acceleration normal to the direction of travel. Traversal of the biarc segmented spiral requires, at each segment junction, infinite jerk normal to the direction of travel. Both demands can not materialise. Actual motions, deemed suitable approximations to the requested motions, are produced as a result of controller intervention. The resulting feed rate and normal acceleration, shown in Figs. 23 and 24, demonstrate less kinematic fluctuation for the path with a higher level of geometric continuity. Less fluctuation implies greater stability. The kinematics resulting from the biarc spiral motion are more predictable in the sense that the kinematics profiles are more characteristic of the schematics developed in section 3. Whether the fluctuations, resulting from the linearly segmented spiral tool path, are significant, is dependent on the application for which the motion is implemented.

The biarc segmented tool path not only produces more stable and predictable motion, but also the actual trajectory of the tool along the path need not deviate from the path specified in the NC file. In order to avoid the infinite normal jerk the tool must simply decelerate in the tangent direction to the tool path. However, in order to traverse the linearly segmented spiral tool path with a continuous feed rate profile, the tool must deviate from the junctions between consecutive linear segments so that the infinite accelerations can be avoided. A smaller positional error between the specified and the actual tool path may therefore be expected for the biarc segmented spiral tool paths.

The characteristic behaviour need not be the same for another machine, for a machine's motion has some dependence on it's own mechatronic attributes. However, through methodology employed in this paper, models of kinematic be-

haviour, with respect to intrinsic shape properties, can be derived. The resulting schematics can be used to inform selection of parameters for given applications. For example, a feed rate may have initially been selected because it results in other desirable conditions, such as particular material removal rates or cutting forces. However, analysis of the shape schematics suggest significant deviation from commanded feed rate may occur at a given region on the tool path, resulting in other undesirable conditions. An informed decision, prior to physical testing, can then be made. A revised feed rate, globally or locally, may be appropriate. Perhaps tool path shape may even be altered to effect kinematics to influence conditions.

This paper only considers planar motion. The investigation may be extended to higher dimensions by considering the effects of torsion. The jerk vector would then gain a binormal component. Incorporating a binormal vector may also provide a means of describing the characteristic nature of motions where a tool's orientation may be allowed to change with respect to the workpiece [41, 42]. This could then motivate the study of the motions of a machine's rotational axes. However, in five-axis machining efforts are usually made to preserve the angles between the cutting tool's rotational axis and the component's surface normal, not the tool path's binormal vector [43]. Further, it can be shown that the geometric properties of a surface can impose impractical kinematic demands on a machine's axes, which in turn can cause surface defects [43]. It then follows that the kinematics imposed by the geometric properties of a surface should be considered as well as the tool paths that lie on it.

7. Concluding remarks

In this paper, constraints were enforced upon the general kinematic vector equations (Eqs. 4, 5 and 6) in order to provide a shape characterisation of tool path motion that accounted for a machines kinematic limits. Two distinct phases of motion originated as a result of deriving the shape characteristic model. It was shown that the velocity limited phase described motion at the

commanded feed rate and the acceleration limited phase described motion with a constant magnitude for the centripetal acceleration vector.

Having postulated a shape characteristic model of tool path motion in section 3, supportive empirical evidence from an example machine (Hermle C600U) was provided. The empirical data demonstrated both the velocity and the acceleration limited phase behaviour as described by the shape schematics.

Performing the free motion tests, detailed in section 4, provides a means of identifying the maximum magnitudes of the kinematic vectors for a tool path of a given shape. From the resulting data, appropriate kinematic constraints may be enforced upon the general kinematic vector equations in order to derive a suitable characterisation of tool path motion. This paper has shown that this approach does not require knowledge of the motion control algorithms implemented on a specific machine's controller. The main advantage of this methodology is that it may be applied to any machine in order to obtain a suitable characterisation of tool path motion.

A given characteristic model depends only upon the shape of a desired tool path and the machine's kinematic limits. These are two of the very few conditions that are identifiable prior to physical machining. The model may therefore be employed in a pre-processing manner to inform the selection of NC file tool path motions. This can therefore help to reduce the material and energy resources being consumed during machining trials and so improve the efficiency and productivity of the manufacturing process.

There are however limitations to the methodology presented in this paper. The kinematic discontinuities inherent in the shape characterisation model and illustrated in the schematics of Figs. 2, 3, 4 and 5, arise from the idealised assumption of removing acceleration and deceleration from and to rest. In practice these discontinuities are not realised. They refer to the discrete time period where the machine transitions from one limited phase to another. The actual curvature at which this transition begins must therefore be less than the theoretical transition curvature. Indeed, this premature transition was shown to occur along the spiral tool paths investigated in section 5. By considering

the nature of a given machine's acceleration and deceleration profiles a given characterisation may be further refined.

References

[1] E. Industries Alliance Standard RS-274-D, Interchangable variable block data format for positioning, contouring, and contouring/positioning numerically controlled machines, Electronic Industries Association.

[2] R. T. Farouki, Y. Tsai, C. S. Wilson, Physical constraints on feedrates and feed accelerations along curved tool paths, Computer Aided Geometric Design 17 (2000) 337–359.

[3] W. Fan, C.-H. Lee, J.-H. Chen, A realtime curvature-smooth interpolation scheme and motion planning for CNC machining of short line segments, International Journal of Machine Tools and Manufacture 96 (2015) 27–46.

[4] S. H. Schot, Jerk: The time rate of change of acceleration, American Journal of Physics 46 (1978) 1090–1094.

[5] S. Tulsyan, Y. Altintas, Local toolpath smoothing for five-axis machine tools, International Journal of Machine Tools and Manufacture 96 (2015) 15–26.

[6] X. Pessoles, Y. Landon, W. Rubio, Kinematic modelling of a 3-axis NC machine tool in linear and circular interpolation, International Journal of Advanced Manufacturing Technology 47 (2010) 639–655.

[7] L. Chanda, R. J. Cripps, Toolpath Geometry and High Speed Machine Axis Motion, Proceedings of the 14th International Conference on Manufacturing Research 3 (2016) 7–12.

[8] X. T. Yan, B. Eynard, C. Jiang, Advanced Design and Manufacture to Gain a Competitive Edge, New Manufactring Techniques and their Role in Improving Enterprise Performance, Springer, 2008.

[9] S. Tajima, B. Sencer, Kinematic corner smoothing for high speed machine tools, International Journal of Machine Tools and Manufacture 108 (2016) 27–43.

[10] R. Bearee, P.-J. Barre, J.-P. Hautier, Vibration reduction abilities of some jerk-controlled movement laws for industrial machines, IFAC Proceedings Volumes 38 (2005) 796–801.

[11] P.-J. Barre, R. Bearee, P. Borne, E. Dumetz, Influence of a jerk controlled movement law on the vibratory behaviour of high-dynamics systems, Journal of Intelligent and Robotic Systems 42 (2005) 275–293.

[12] M. T. Lin, M. S. Tsai, H. T. Yau, Development of a dynamics-based NURBS interpolator with real-time look-ahead algorithm, International Journal of Machine Tools and Manufacture 47 (2007) 2246–2262.

[13] K. Erkorkmaz, Y. Altintas, High speed CNC system design. Part I: jerk limited trajectory generation and quintic spline interpolation, International Journal of Machine Tools and Manufacture 41 (2001) 1323–1345.

[14] S. J. Yutkowitz, W. Chester, Apparatus and Method for Smooth Cornering in a Motion Control System (2005).

[15] B. Sencer, K. Ishizaki, E. Shamoto, A curvature optimal sharp corner smoothing algorithm for high-speed feed motion generation of NC systems along linear tool paths, International Journal of Advanced Manufacturing Technology 76 (2015) 1977–1992.

[16] H. Zhao, L. Zhu, H. Ding, A real-time look ahead interpolation methodology with curvature-continuous b-spline transition scheme for CNC machining of short line segments, International Journal of Machine Tools and Manufacture 65 (2013) 88–98.

[17] V. Pateloup, E. Duc, P. Ray, B-spline approximation of circle arc and straight line for pocket machining, Computer Aided Design 42 (2010) 817–827.

[18] G. Farin, Curves and Surfaces for CAGD, Morgan Kaufmann Publishers, 2002.

[19] Y. Jin, Y. He, J. Fu, Z. Lin, W. Gan, A fine-interpolation-based parametric method with a novel real-time look-ahead algorithm, Computer-Aided Design 55 (2014) 37–48.

[20] M. M. Lipschutz, Differential Geometry, McGraw-Hill, 1969.

[21] M. R. Spiegel, Theory And Problems Of Vector Analysis and an Introduction to Tensor Analysis, McGraw-Hill, 1988.

[22] P.-B. Barre, R. Bearee, P. Borne, E. Dumetz, Inuence of a Jerk Controlled Movement Law on the Vibratory Behaviour of High-Dynamics Systems, Journal of Intelligent and Robotic Systems 42 (2005) 275–293.

[23] S. Tajima, B. Sencer, Global tool-path smoothing for CNC machine tools with uninterrupted acceleration, International Journal of Machine Tools and Manufacture 121 (2017) 81–95.

[24] Z. Jia, D. Song, J. Ma, G. Hu, W. Su, A NURBS interpolator with constant speed at feedrate-sensitive regions under drive and contour-error constraints, International Journal of Machine Tools and Manufacture 116 (2017) 1–17.

[25] Y. Wang, D. Yang, R. Gai, S. Wang, S. Sun, Design of trigonometric velocity scheduling algorithm based on pre-interpolation and look-ahead interpolation, International Journal of Machine Tools and Manufacture 96 (2015) 94–105.

[26] S. H. Schot, Aberrancy: Geometry of the third derivative, Mathematics Magazine 51 (1978) 259–275.

[27] A. Hermle, Hermle C600 series brochure, Gosheim Germany, 1999.

[28] C. S. Smith, Piezoresistance effect in germanium and silicon, Physical Review 94 (1954) 42–49.

[29] K. J. Vinoy, G. K. Ananthasuresh, R. Pratap, S. B. Krupanidhi, Mirco and Smart Devices and Systems, Springer, 2014.

[30] T. R. Padmanabhan, Industrial Instrumentation: Principles and Design, Springer, 2000.

[31] HBM Test and Measurement, *eDAQ-lite System*, [Online]. Available from: `https://www.hbm.com/en/5502/daq-data-acquisition-systems`, [Accessed 15th November 2017].

[32] HBM Test and Measurement, *SoMat Test Control Environment Software*, [Online]. Available from: `https://www.hbm.com/en/1996/software/`, [Accessed 15th November 2017].

[33] C. Cadwallader, Delcam incorporates machine DNA profiler into PowerMill 2013, Machinery, 2012.

[34] S. W. Mackman, W. Strother, S. Hobbs, Method and system for testing a machine tool GB patent (2012).

[35] S. W. Mackman, W. Strother, S. Hobbs, Method and system for testing a machine tool US patent (2013).

[36] E. M. Stein, G. Weiss, Introduction to Fourier Analysis on Euclidean Spaces, Princeton University Press, 1971.

[37] J. M. Ali, R. M. Tookey, J. V. Ball, A. A. Ball, The generalised Cornu spiral and its application to span generation, Journal of Computational and Applied Mathematics 107 (1999) 37–47.

[38] W. H. Press, S. A. Teukolsky, W. T. Vetterling, B. P. Flannery, Numerical Recipes in C, The art of scientific computing, Cambridge University Press, 1994.

[39] A. W. Nutbourne, P. M. McLellan, R. M. L. Kensit, Curvature profiles for planes curves, Computer Aided Design 4 (1972) 176–184.

[40] K. M.Bolton, Biarc curves, Computer-Aided Design 7 (1975) 89–92.

[41] R. J. Cripps, G. Mullineux, Constructing 3D motions from curvature and torsion profiles, Computer-Aided Design 11 (2012) 379–387.

[42] R. J. Cripps, G. Mullineux, Using geometric algebra to represent and interpolate tool poses, International Journal of Computer Integrated Manufacturing 29 (2016) 406–423.

[43] R. J. Cripps, B. Cross, G. Mullineux, M. Hunt, Machinability of Surfaces via Motion Analysis, Mathematical Methods for Curves and Surfaces MMCS 2016 Lecture Notes in Computer Science 10521 (2017) 74–95.

[44] D. Kincaid, W.Cheney, Numerical Analysis: Mathematics of Scientific Computing, Brooks/Cole, 1996.

Appendix A. Sampling Period, T_s

Sampling period, T_s, is the time interval in which a controller receives position feedback from servo loops. Since the purpose of the investigation is to study the effects of shape on tool path motion, care has been taken to ensure that tool path motions do not require processing speeds greater than the controller's processing capability.

The greater the number of points used to define a tool path, the greater the processing speed required from the controller. Consider a planar linear tool path defined by N equally spaced points. If the commanded feed rate is achieved, the distance between consecutive points does not require a sampling period greater than the controller's limit. By incrementally increasing the number of equally spaced points until the commanded feed rate is not achieved, the controller sampling period can be identified.

A planar linear path has no curvature and no torsion, so shape has no affect. The length of the line does however affect the achieved feed rate. The length of the line should be sufficiently long such that the machine can accelerate to the

commanded feed rate from rest and decelerate from the commanded feed rate to rest.

The specific values of feed rate and line length chosen are immaterial. In general, the greater the commanded feed rate, the greater the distances required for acceleration and deceleration and so the longer the line needed. However, for a line of a given length, the greater the commanded feed rate, the fewer equally spaced points required to observe a difference between the commanded and achieved feed rates.

The Hermle's maximum permissible feed rate, F_{max}, $(0.6m/s)$ is therefore set as the commanded feed rate in the linear tool path motion tests. The tool path length is set to $0.5m$, as preliminary testing showed such a length is sufficiently long to enable the commanded feed rate to be achieved. By incrementally increasing the density of the equally spaced points, it is found that the threshold number of points, N_t, at which the specified feed rate is still achieved is 214 (Fig. A.25). From this, the minimum distance between consecutive points can be found, $s_{min} = L/N_t$. It then follows that $T_s = s_{min}/F$.

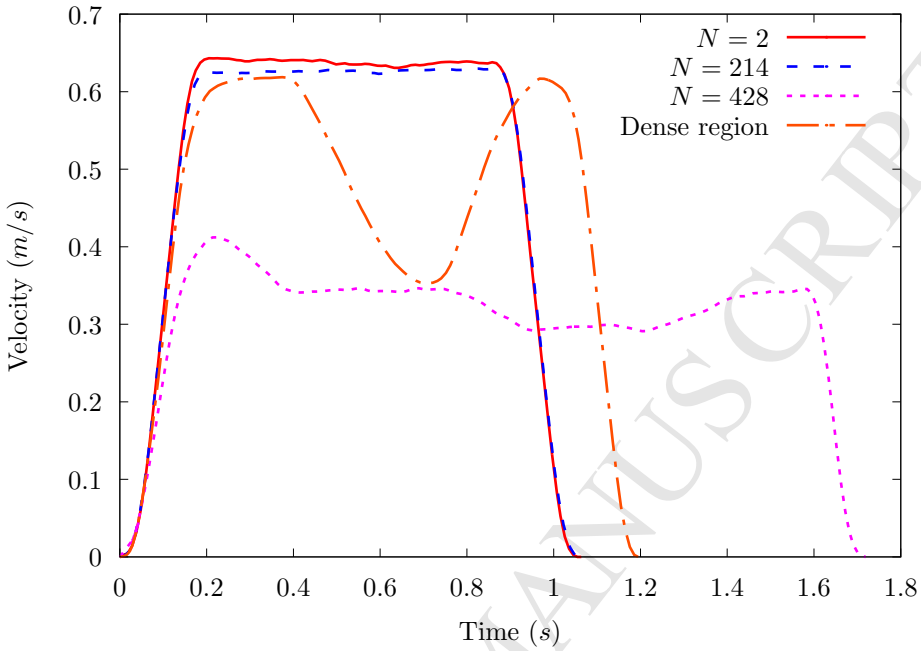

Figure A.25: Feed rate profiles for different point densities

To verify the threshold number of points does not affect motion, a comparison is made to a motion produced for $N = 2$ points (start and end points of the line). Fig. A.25 suggests negligible difference between the two motions. Doubling the threshold number of points to 428, halves the distance between consecutive points and the achieved feed rate is approximately halved (Fig. A.25). Further, the line is then divided into three sections, the first and last sections contain points minimally spaced and the middle section contains points that are spaced with half the minimal distance. From the figure it can be seen that the achieved feed rate drops to approximately half in the middle dense region as the sampling period phenomenon takes effect.

Appendix B. Jerk vector derivation

Taking the derivative of Eq. (5) with respect to time, provides an expression for the jerk vector:

$$\mathbf{j}(t) = \frac{d}{dt}\left[\frac{d^2s}{dt^2}\hat{\mathbf{t}}(s) + \left\{\frac{ds}{dt}\right\}^2 \kappa(s)\hat{\mathbf{n}}(s)\right]$$

$$= \frac{d}{dt}\left[\frac{d^2s}{dt^2}\hat{\mathbf{t}}(s)\right] + \frac{d}{dt}\left[\left\{\frac{ds}{dt}\right\}^2 \kappa(s)\hat{\mathbf{n}}(s)\right] .$$

Let

$$\xi_0(t) \equiv \frac{d}{dt}\left[\frac{d^2s}{dt^2}\hat{\mathbf{t}}(s)\right]$$

and

$$\xi_1(t) \equiv \frac{d}{dt}\left[\left\{\frac{ds}{dt}\right\}^2 \kappa(s)\hat{\mathbf{n}}(s)\right] .$$

It then follows that,

$$\xi_0(t) = \frac{d^3s}{dt^3}\hat{\mathbf{t}}(s) + \frac{ds}{dt}\frac{d^2s}{dt^2}\frac{d\hat{\mathbf{t}}(s)}{ds}.$$

Substituting Eq. (1) into the above equation gives

$$\xi_0(t) = \frac{d^3s}{dt^3}\hat{\mathbf{t}}(s) + \frac{ds}{dt}\frac{d^2s}{dt^2}\kappa(s)\hat{\mathbf{n}}(s) . \tag{B.1}$$

Also,

$$\xi_1(t) = 2\frac{ds}{dt}\frac{d^2s}{dt^2}\kappa(s)\hat{\mathbf{n}}(s) + \left\{\frac{ds}{dt}\right\}^3 \frac{d}{ds}\left[\kappa(s)\hat{\mathbf{n}}(s)\right]$$

$$= 2\frac{ds}{dt}\frac{d^2s}{dt^2}\kappa(s)\hat{\mathbf{n}}(s) + \left\{\frac{ds}{dt}\right\}^3 \frac{d\kappa(s)}{ds}\hat{\mathbf{n}}(s) + \left\{\frac{ds}{dt}\right\}^3 \kappa(s)\frac{d\hat{\mathbf{n}}(s)}{ds} .$$

Substituting Eq. (2) into the above equation gives,

$$\xi_1(t) = 2\frac{ds}{dt}\frac{d^2s}{dt^2}\kappa(s)\hat{\mathbf{n}}(s) + \left\{\frac{ds}{dt}\right\}^3 \frac{d\kappa(s)}{ds}\hat{\mathbf{n}}(s) - \left\{\frac{ds}{dt}\right\}^3 \{\kappa(s)\}^2\hat{\mathbf{t}}(s) + \left\{\frac{ds}{dt}\right\}^3 \tau(s)\kappa(s)\hat{\mathbf{b}}(s) . \tag{B.2}$$

Summing Eq. (B.1) and Eq. (B.2) produces the equation given below,

$$\mathbf{j}(t) = j_t(t)\hat{\mathbf{t}}(s) + j_n(t)\hat{\mathbf{n}}(s) + j_b(t)\hat{\mathbf{b}}(s) \ ;$$

where

$$j_t(t) = \frac{d^3s(t)}{dt^3} - \left\{\frac{ds(t)}{dt}\right\}^3 \{\kappa(s)\}^2 \ ,$$

$$j_n(t) = 3\frac{ds(t)}{dt}\frac{d^2s(t)}{dt^2}\kappa(s) + \left\{\frac{ds(t)}{dt}\right\}^3 \frac{d\kappa(s)}{ds} \ ,$$

and

$$j_b(t) = \left\{\frac{ds(t)}{dt}\right\}^3 \kappa(s)\tau(s) \ .$$

Appendix C. Derivation of the third derivative of arc length with respect to time

Taking the derivative of Eq. (12) with respect to time gives,

$$\begin{aligned} \frac{d^3s}{dt^3} &= -\frac{1}{2}\Psi_2 \frac{d}{ds}\left[\frac{1}{\{\kappa(s)\}^2}\frac{d\kappa(s)}{ds}\right]\frac{ds}{dt} \\ &= -\frac{1}{2}\Psi_2 \frac{1}{\{\kappa(s)\}^2}\left[\frac{d^2\kappa(s)}{ds^2} - 2\frac{1}{\kappa(s)}\left\{\frac{d\kappa(s)}{ds}\right\}^2\right]\frac{ds}{dt} \ . \end{aligned} \tag{C.1}$$

An alternative form of Eq. (10) is

$$\frac{ds}{dt} = \frac{\sqrt{\Psi_2}\sqrt{\kappa(s)}}{\kappa(s)} \ . \tag{C.2}$$

Substituting Eq. C.2 into Eq. (C.1) gives,

$$\frac{d^3s}{dt^3} = -\frac{1}{2}\Psi_2\sqrt{\Psi_2}\sqrt{\kappa(s)}\frac{1}{\{\kappa(s)\}^3}\left[\frac{d^2\kappa(s)}{ds^2} - 2\frac{1}{\kappa(s)}\left\{\frac{d\kappa(s)}{ds}\right\}^2\right] \ .$$

Appendix D. Numerical integration error bound

For a given interval $[s_{min}, s_{max}]$, the total error ε_T of numerical integration, using the trapezoidal rule, can be given as

$$\varepsilon_T = -\frac{(s_{max} - s_{min})^3}{12N^2} \frac{\sum_{i=0}^{N-1} f''(\zeta_i)}{N} \ ,$$

where N is the number of segments in the interval and $f''(\zeta_i)$ is the second derivative of the integrand evaluated at some point ζ_i, $s_{min} \leq \zeta_i \leq s_{max}$ [44]. The expression

$$\frac{\sum_{i=0}^{N-1} f''(\zeta_i)}{N} \ ,$$

can be considered as an approximate average value of the second derivative in the specified interval. At some point, the second derivative will take its average value ζ_{avg}, assuming it is continuous. In the case of the integrands given in Eqs. (16) and (17), it is shown below in Eqs. (D.3) and (D.4) and Fig. D.26 that the second derivatives are indeed continuous. Therefore let,

$$\zeta_{avg} = \frac{\sum_{i=0}^{N-1} f''(\zeta_i)}{N} \ .$$

The total error may then be expressed as

$$\varepsilon_T = -\frac{(s_{max} - s_{min})^3}{12N^2} \zeta_{avg} \ .$$

It is not known where ζ_{avg} lies in the interval. By replacing ζ_{avg} with $max(|f''(\zeta_i)|)$, an upper bound ε_B on the total error for the given interval can be found. It then follows that,

$$\varepsilon_B = -\frac{(s_{max} - s_{min})^3}{12N^2} max(|f''(\zeta_i)|) \ . \tag{D.1}$$

The above equation shows that to identify error bounds of the Cornu spiral positions, resulting from Eqs. (16) and (17), evaluation of the second derivatives of the corresponding integrands is required. This can be achieved by rewriting Eqs. (16) and (17) as

$$x(s) = x_0 + \int_0^s f_x(\sigma) d\sigma \ ,$$

and

$$y(s) = y_0 + \int_0^s f_y(\sigma) d\sigma \ ,$$

where $f_x(\sigma) = cos(\alpha(\sigma))$, $f_y(\sigma) = sin(\alpha(\sigma))$ and

$$\alpha(\sigma) = \theta_0 + \frac{1}{2L}\{2\kappa_0 L\sigma + (\kappa_1 - \kappa_0)\sigma^2)\} \ . \tag{D.2}$$

The first and second derivatives of the integrand $f_x(\sigma)$ are

$$\frac{df_x(\sigma)}{d\sigma} = -\frac{d\alpha(\sigma)}{d\sigma} sin(\alpha(\sigma)) \ ,$$

and

$$\frac{d^2 f_x(\sigma)}{d\sigma^2} = -\left[\frac{d^2\alpha(\sigma)}{d\sigma^2} sin(\alpha(\sigma)) + \left\{\frac{d\alpha(\sigma)}{d\sigma}\right\}^2 cos(\alpha(\sigma))\right] \ , \tag{D.3}$$

respectively. Similarly,

$$\frac{df_y(\sigma)}{d\sigma} = \frac{d\alpha(\sigma)}{d\sigma} cos(\alpha(\sigma)) \ ,$$

and

$$\frac{d^2 f_y(\sigma)}{d\sigma^2} = \frac{d^2\alpha(\sigma)}{d\sigma^2} cos(\alpha(\sigma)) - \left\{\frac{d\alpha(\sigma)}{d\sigma}\right\}^2 sin(\alpha(\sigma)) \ . \tag{D.4}$$

From Eq. (D.2) it follows that,

$$\frac{d\alpha(\sigma)}{d\sigma} = \frac{1}{L}\{\kappa_0 L + (\kappa_1 - \kappa_0)\sigma\} \ ,$$

and

$$\frac{d^2\alpha(\sigma)}{d\sigma^2} = \frac{\kappa_1 - \kappa_0}{L} \ .$$

$|cos(\alpha(\sigma))|$ and $|sin(\alpha(\sigma))| \leq 1, \forall\, \sigma$, $d^2(\alpha(\sigma))/d\sigma^2$ is constant, and $\{d\alpha(\sigma)/d\sigma\}^2 = O(\sigma^2)$ since,

$$\left\{\frac{d\alpha(\sigma)}{d\sigma}\right\}^2 = \frac{1}{L^2}\{\kappa_0 L + (\kappa_1 - \kappa_0)\sigma\}^2 \ . \tag{D.5}$$

It then follows that the magnitude of $\{d\alpha(\sigma)/d\sigma\}^2$ increases monotonically and so its maximum value occurs at s_{max} for the interval $[s_{min}, s_{max}]$. As illustrated by Fig. D.26, as $\sigma \to \infty$, $\{d\alpha(\sigma)/d\sigma\}^2$, denoted $(\alpha')^2$ in Fig. D.26, begins to envelope both second derivative terms (Eqs. (D.3) and (D.4)). By substituting Eq. (D.5) into Eq. (D.1) an alternative expression for the error bound can be formed

$$\varepsilon_B = -\frac{(s_{max} - s_{min})^3\{\kappa_0 L + (\kappa_1 - \kappa_0)s_{max}\}^2}{12N^2L^2} \ .$$

The number of segments required, for a given interval, to obtain a suitable magnitude of error can then be identified,

$$N = \sqrt{\frac{(s_{max} - s_{min})^3\{\kappa_0 L + (\kappa_1 - \kappa_0)s_{max}\}^2}{12|\varepsilon_B|L^2}} \ .$$

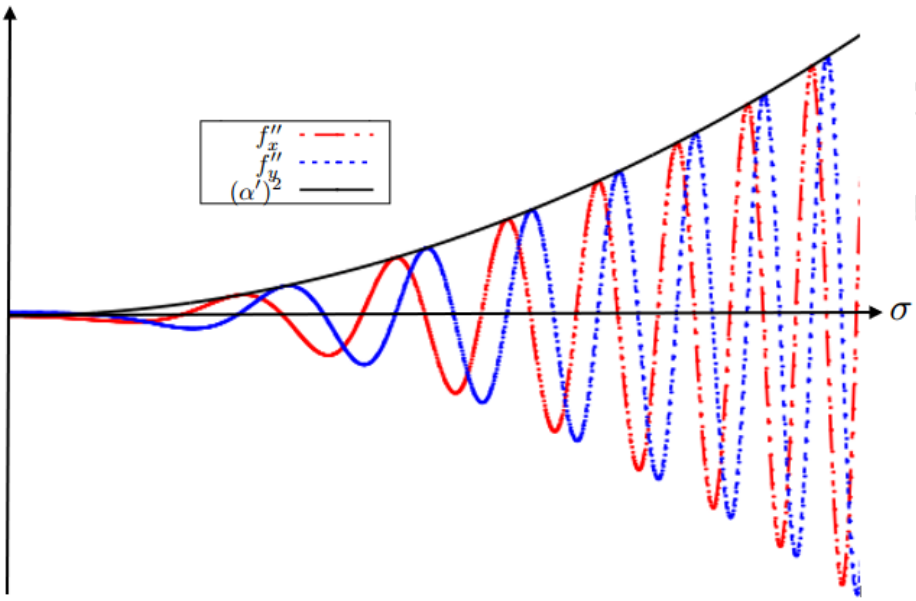

Figure D.26: Error bound

No acknowledgments required.

Highlights (for review)

By performing free motion tests on a machine's axes it is possible to identify the maximum magnitudes of the kinematic vectors for a tool path of a given shape. From the resulting data, appropriate kinematic constraints are enforced upon the general kinematic vector equations to derive a suitable characterisation of tool path motion. The paper shows that this approach does not require knowledge of the motion control algorithms implemented on a given machine's controller. The main advantage of this methodology is that it may be applied to any machine in order to obtain a suitable characterisation of tool path motion.